

THESIS FOR THE DEGREE OF LICENTIATE OF ENGINEERING

Enzyme Immobilization in Mesoporous Silica

HANNA GUSTAFSSON



CHALMERS

Department of Chemical and Biological Engineering
CHALMERS UNIVERSITY OF TECHNOLOGY
Göteborg, Sweden
2012

Enzyme Immobilization in Mesoporous Silica

HANNA GUSTAFSSON

© HANNA GUSTAFSSON, 2012

Licentiatuppsatser vid Institutionen för kemi- och bioteknik
Chalmers tekniska högskola
Serie Nr: 2012:2
ISSN 1652-943X

Department of Chemical and Biological Engineering
Chalmers University of Technology
SE-412 96 Göteborg
Sweden

Telephone +46 (0)31-772 1000

Printed by Chalmers Reproservice

Göteborg, Sweden, 2012

Enzyme Immobilization in Mesoporous Silica

HANNA GUSTAFSSON

Department of Chemical and Biological Engineering
Chalmers University of Technology

ABSTRACT

Catalysts are widely used in many industries for production of chemicals, pharmaceuticals, fuels and energy. There is a need for more sustainable production processes, with reduced energy and raw material consumption together with a reduction in waste and toxic by-products. Conventional synthetic catalysts often demand harsh chemical conditions and multi-step processes. Biocatalysts, i.e., enzymes, have high substrate specificity and good catalytic efficiency under mild reaction conditions and are therefore alternatives to synthetic catalysts. Immobilization on a solid support is a method to overcome limitations, such as low long-term stability and poor reusability of the enzymes. Mesoporous silica is a promising material for this purpose. The large surface area and the well-ordered and uniform pores make them suitable as hosts for enzymes.

This thesis describes the immobilization of four types of hydrolytic enzymes into mesoporous silica with varying pore size, particle size and morphology. The pH during the immobilization was also varied in order to find the most optimal conditions for high loading, proper stability and good catalytic activity.

Mesoporous silica with hexagonally ordered and narrow pore size distribution was synthesized (SBA-15). Three pore sizes, 5, 6 and 9 nm, were obtained by varying the hydrothermal temperature. The particles were rod-shaped, about 2 μm in length, and somewhat agglomerated. Three types of silica particles with varying size and morphology but with the same pore size (9 nm) were also synthesized. Two of them were obtained by modifying the synthesis conditions of conventional SBA-15; one type being broad and about 1 μm long, the other more rod-shaped and about 300 nm long. By decreasing the stirring time during the condensation, particle agglomeration could be avoided. The third particle type was synthesized by forming a composite material with silica and polystyrene clusters inside the droplets of an oil-in-water emulsion (HMM). Spherical, 40 nm small particles with non-ordered pores and a wide pore size distribution were obtained. The materials have been characterized with electron microscopy, nitrogen sorption and small angle X-ray scattering.

Trypsin from *bovine pancreas* (BPT) was immobilized yielding a rapid and large loading. The optimal pore size was found to be 6 nm. A larger pore size gave less protection against autolysis and a smaller pore diameter turned out to be too narrow. *Mucor miehei* lipase (MML) was immobilized at a lower rate and also gave lower loading, probably due to a larger molecular size and an unfavorable surface charge. The 9 nm pores provided the largest loading and the highest activity. The immobilized lipase was more active compared to free lipase, most likely because of interfacial activation at the silica surface. The highest lipase activity was found in the medium sized particles; however, the loading did not differ significantly between the particles with varying sizes. Hindered substrate diffusion in the large particles and a very wide pore size distribution in the small particles can explain the difference in activity. Lipase should be immobilized in its most active state, which was found to be at pH 8. Immobilization of feruloyl esterases (FAE) resulted in a desired altered enzymatic activity towards transesterification compared to the use of free enzyme in solution. The immobilization was rapid and the stability and reusability was good.

Keywords: Mesoporous, silica, pore size, particle morphology, immobilization, encapsulation, enzyme, lipase, trypsin, feruloyl esterase

List of publications

This thesis is a summary of the following papers:

- I. A comparison of lipase and trypsin encapsulated in mesoporous materials with varying pore sizes and pH conditions
Hanna Gustafsson, Christian Thörn and Krister Holmberg
Colloids and Surfaces B: Biointerfaces 87 (2011) 464– 471
- II. Immobilization of lipase from *Mucor miehei* and *Rhizopus oryzae* into mesoporous silica
-The effect of varied particle size and morphology
Hanna Gustafsson, Emma Johansson, Albert Barrabino and Krister Holmberg
Submitted to *Microporous and Mesoporous Materials*
- III. Immobilization of feruloyl esterases in mesoporous materials leads to improved transesterification yield
Christian Thörn, Hanna Gustafsson and Lisbeth Olsson
Journal of Molecular Catalysis B: Enzymatic 72 (2011) 57– 64

Contribution report to the listed publications

- I. Responsible for experimental outline, experimental work and for writing the major part of the manuscript.
- II. Responsible for experimental outline and experimental work except synthesis of the MPS-300 and MPS-40 silica particles. Responsible for writing the major part of the manuscript.
- III. Responsible for synthesis and characterization of the mesoporous materials.

TABLE OF CONTENTS

1 INTRODUCTION	1
2 MESOSTRUCTURED MATERIALS	3
2.1 Mesoporous silica	3
2.1.1 SBA-15	6
2.1.2 HMM	7
3 IMMOBILIZATION OF ENZYMES	9
3.1 Use of mesoporous silica for enzyme immobilization	9
3.1.1 Immobilization methods	10
3.1.2 Support properties	12
3.2 Enzymes	12
3.2.1 Lipase	12
3.2.2 Trypsin	14
3.2.3 Feruloyl esterases	14
4 ANALYTICAL TECHNIQUES	17
4.1 Transmission electron microscopy	17
4.2 Scanning electron microscopy	17
4.3 Physisorption	18
4.4 Small angle X-ray scattering	20
4.5 UV/Vis spectrometry	21
4.5.1 Enzyme activity	22
4.5.2 Protein concentration	22
4.6 Optical tensiometry	24
5 RESULTS AND DISCUSSION	25
5.1 Characterization of mesoporous silica	25
5.2 Immobilization of enzymes in mesoporous silica	30
5.2.1 Enzyme loading	30
5.2.2 Enzyme leakage	33
5.3 Catalytic activity of immobilized enzymes	34

6 CONCLUDING REMARKS AND FUTURE WORK	39
ACKNOWLEDGEMENT	41
REFERENCES	43

Chapter 1

INTRODUCTION

In the chemical and pharmaceutical industries there is a need for more sustainable production processes, with reduced energy and raw material consumption together with a reduction in waste and toxic by-products. Catalysts are widely used in industrial processes to improve and speed up the reactions. Conventional synthetic catalysts used in industry often demand harsh chemical conditions and multi-step processes, leading to excessive energy consumption and generation of much waste. By replacing synthetic catalysts with enzymes cleaner products and processes can be achieved [1,2]. Enzymes are biological catalysts found in all living organisms. They have a high catalytic efficiency, substrate specificity and selectivity under mild reaction conditions with low energy requirements. Due to the substrate specificity multi-step processes can often be reduced to one single step, resulting in less by-product formation [3]. Enzymes can also catalyze the synthesis of high value, optically active compounds that cannot be produced by conventional catalysts [4]. Furthermore, advances in protein engineering, like site-directed mutagenesis, have made it possible to manipulate the enzyme properties to yield an even more efficient synthesis [5].

However, there are also limitations in using enzymes in large-scale production such as high cost and lack of long-term operational stability. It is difficult to separate them from the reaction system, which limits the recovery of the enzyme and may lead to contamination of the final product. These disadvantages can be overcome by immobilization of the enzyme; immobilized enzymes are often more stable and more easy to recover than enzymes free in solution [6,7]. Additionally, enzyme immobilization may improve the catalytic activity [8]. There are several immobilization methods available, including binding of the enzyme to a solid support, encapsulation inside a material or cross-linking the enzyme into large aggregates [6,9]. Binding of the enzyme to a support through physical adsorption is the most simple immobilization method and therefore also frequently used in large-scale production [10].

A promising material as support for enzymes is mesoporous silica. The large surface area and the well-ordered and uniform pores with an adjustable pore size, typically in the size range of 2 to 15 nm, make them suitable for biomolecules, like enzymes [11,12]. Compared to a flat surface the porous structure enables a large quantity of enzyme to be immobilized. Moreover, mesoporous silica is a structurally robust material, chemically stable over a broad pH and temperature range. The materials are made by a templating procedure, using an organic template that is subsequently removed by solvent extraction or by calcination or by a combination of these. The pore

dimension can be tailored with high precision by the choice of templating molecule and by the synthesis conditions.

The main objective of this work is to immobilize enzymes into mesoporous silica through physical adsorption and to study the influence of varying pore size, particle size and particle morphology on the loading capacity, catalytic activity and reusability of the immobilized enzyme. The goal is to obtain a stable system, where the enzyme is properly retained inside the material with minimal leaching while maintaining a high and stable catalytic activity. The variations in enzyme characteristics are also investigated and correlated to the properties of the mesoporous silica material. The long term goal is to develop a procedure for immobilizing enzymes that can be used in industry for more sustainable chemical processes.

The thesis is built on three papers where Paper I deals with the immobilization of two hydrolytic enzymes, trypsin from *bovine pancreas* (BPT) and lipase from *Mucor miehei* (MML) into mesoporous silica with varying pore size. The two enzymes were compared with regard to size, surface charge and catalytic performance. In Paper II mesoporous silica with varying particle size and morphology were synthesized. Two lipases, MML and lipase from *Rhizopus oryzae* (ROL) were immobilized and the effect of the particle properties on the loading and the activity was studied. In Paper III feruloyl esterase (FAE) was immobilized into the silica nanopores and the effect of the confinement on the activity was investigated.

Chapter 2

MESOSTRUCTURED MATERIALS

Mesoporous materials are defined as inorganic solids with a pore size range of 2-50 nm. They can have a large variety of properties with respect to composition, pore shape and particle morphology to name a few. Most mesoporous materials are oxides, such as SiO₂, Al₂O₃, TiO₂ and ZrO₂ and the structure is usually cubic or hexagonal [13-15]. Mesoporous silica has been used in this work and is the only material described here. They were discovered in the early 90's [11,16,17] and soon became the topic of much research, with focus on either synthesis, characterization or applications. The robust and thermally stable structures together with a large surface area, tunable pore size, and well-ordered and uniform pores, make them suitable as supports in drug delivery [18,19], separation [20], catalysis [21] and biocatalysis [10,22-24].

2.1 Mesoporous silica

Mesoporous silica is obtained from the organic-inorganic self-assembly driven by weak non-covalent bonds such as hydrogen bonds, van der Waals attractions and electrostatic interactions between a surfactant, called template, and an inorganic species. The surfactant can be either cationic, like CTAB [25], or nonionic, usually a block copolymer [12], and is dissolved in an aqueous solution. Due to their amphiphilicity, the surfactant will form aggregates, called micelles, above the critical micelle concentration (CMC). The hydrophilic group is facing the solvent whereas the hydrophobic tail is situated inside the micelle in order to minimize contact with the water. The aggregate structure primarily depends on the structure of the surfactant and is determined by the critical packing parameter (CPP). The CMC also depends on the solution conditions, such as temperature and salt concentration.

$$CPP = \frac{v}{l \cdot a} \quad (1)$$

where v is the volume of the hydrophobic chain, l the length of the hydrophobic tail, and a the cross sectional area of the hydrophilic part. By varying the size or length of the hydrophilic or hydrophobic groups, micelles of different size and shape can be obtained. Figure 1 illustrates the relation between CPP and various aggregate structures.

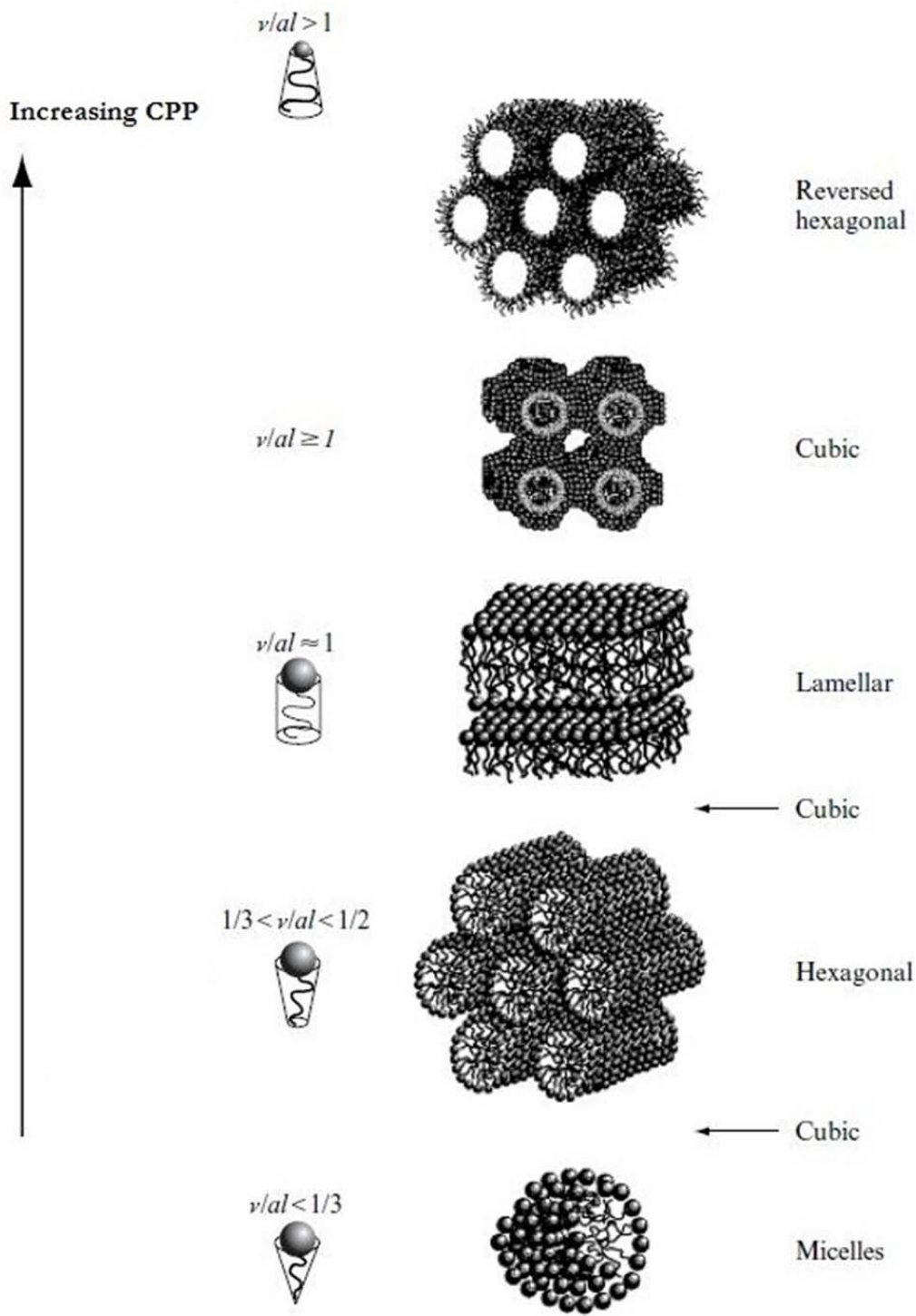


Figure 1. Critical packing parameters and the corresponding aggregate structures. Redrawn from Holmberg et al., *Surfactants and Polymers in Aqueous Solution*: 2nd ed. [26].

A silica precursor is added to the micellar solution. This precursor is either an alkoxide, for example tetraethyl orthosilicate (TEOS) (Figure 2) or an inorganic salt such as sodium silicate. In this work, only TEOS has been used as silica precursor.

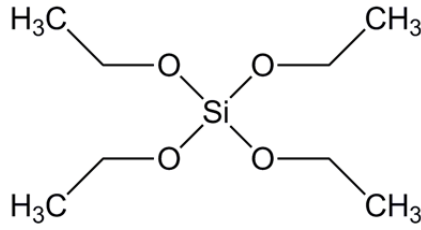
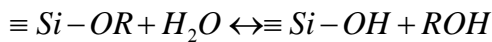


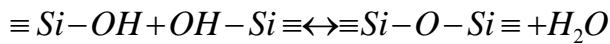
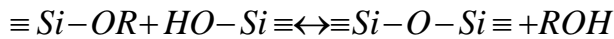
Figure 2. Tetraethyl orthosilicate (TEOS).

An alkoxide hydrolyses under acidic or basic conditions followed by condensation and polymerization, forming a silica network around the template. The different reactions take place simultaneously. Acidic conditions promote the hydrolysis reaction whereas basic conditions result in fast condensation reactions [27].

Hydrolysis:



Condensation:



After the reaction is finished the formed material can be hydrothermally treated for further cross-linking, reorganization and particle growth [12]. There are several factors that affect particle growth and the final particle morphology in addition to the hydrothermal treatment. Additives such as cosolvents, cosurfactants, inorganic salts etc., variation of the pH, and change of the type and amount of the template surfactant are ways to control the morphology, yielding for example mesostructured silica fibers, single rods, platelets, gyroids and spheres [28-32].

The hydrophobic part of the surfactant molecule determines the pore size. In general, a large hydrophobic group generates a larger pore size. Additional ways to tune the pore size of the mesoporous materials is to add an organic swelling agent that is solubilized in the hydrophobic core leading to swelling of the micelle [12,33]. The pore size can also be adjusted by varying the temperature during the hydrothermal treatment (see Section 2.1.1) [12,34]. After preparation of the organic-inorganic hybrid material, the surfactant template is removed by calcination, which is the most common method, or extraction, resulting in a mesoporous material. During calcination the temperature is slowly elevated and kept constant for several hours to completely remove all organic material. One drawback with calcination is that many of the silanol groups on the silica surface are converted into siloxane bridges, which have a hydrophobic character [35,36]. Extraction with for example ethanol [14] is a milder method to remove the template but the

drawback with this procedure is that surfactant residues may remain inside the pores. This is typically a problem when block copolymers are used as template. The PEO chains cause formation of micropores in the corona [37].

In Papers I and III SBA-15 [14] was synthesized with varying pore size. In Paper II SBA-15 with varying particle size and morphology was synthesized together with HMM [38]. SBA-15 has highly uniform, hexagonally ordered, cylindrical pores and the pore size can be controlled in the range of 6-15 nm. HMM materials have non-ordered pores with a tunable pore size between 4 and 15 nm and a particle diameter in the range of 20-80 nm.

2.1.1 SBA-15

SBA-15 (Santa Barbara Amorphous) is a hexagonally ordered mesoporous silica material with cylindrical pores and a rather large pore diameter. They are synthesized under acidic conditions using a nonionic triblock copolymer, often referred to as Pluronic after the BASF trade name, as template. A Pluronic consists of two hydrophilic polyethylene oxide chains (PEO) with one hydrophobic polypropylene oxide chain (PPO) in between. Figure 3 shows Pluronic P123, which is used in this study. The hydrophilic groups are each 20 units long and the hydrophobic group is 70 units long. When forming micelles in an aqueous solution the PPO group will be situated in the center of the micelles, called the core and the PEO groups will be facing the solution in the micelle corona.

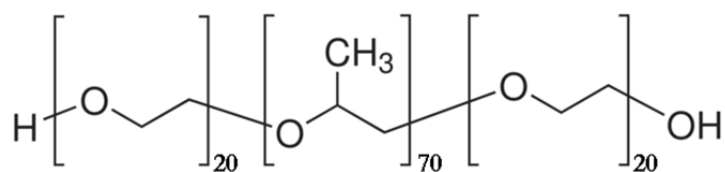


Figure 3. The block copolymer surfactant Pluronic P123.

A large number of studies have been focusing on the synthesis mechanism and formation pathway for mesoporous silicates. The initial formation mechanism of hexagonally ordered material, suggested by Beck et al. (Figure 4), includes many possibilities where two of the main pathways are the “*liquid crystal templating*” process and the “*cooperative self-assembly*” process [25]. Briefly, the “*liquid crystal templating*” process includes organization of surfactant molecules into hexagonally arranged liquid crystals followed by silica condensation around the elongated micelles whereas the “*cooperative self-assembly*” is based on the interactions between silicates and surfactants to form inorganic-organic mesostructured composites. Studies on the formation mechanism of SBA-15 show that the micelles are initially spherical before addition of the silica precursor. The hydrophobic silica precursor first enters the micelle core. When the siliceous species hydrolyze they migrate out of the micelle core and attach to the hydrophilic part of the surfactant, in the micelle corona. As shown in Section 2.1 the hydrolysis and the condensation of TEOS generate ethanol. The PPO chains are soluble in ethanol in a certain temperature range leading to

migration of ethanol into the hydrophobic core. This leads to a volume expansion of the core and to a CPP increase, which results in a sphere-to-rod transition of the micelle (see Equation 1 and Figure 1) [39]. The silica polymerization causes attractive interactions between the micelles which leads to micelle flocculation and rearrangement into hexagonally ordered structures [40-42].

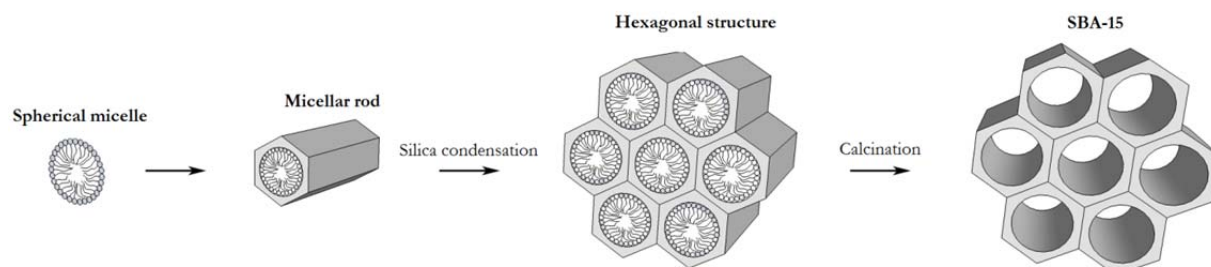


Figure 4. Proposed formation mechanism of SBA-15.

After formation of hexagonally ordered structures the material is further reorganized and cross-linked by the hydrothermal treatment. The pore size is tuned by varying the temperature during the aging process. When the temperature is increased the PEO groups are partially dehydrated and become more hydrophobic. The PEO groups are retracted from the silica network into the hydrophobic core, thereby increasing the pore size [34]. Finally, the block copolymer is removed by calcination resulting in a mesoporous material with hexagonally ordered pores.

The most common particle morphology for SBA-15 is rods grown together in fibers [12]. Addition of an inorganic salt and/or decreasing the stirring time generates discrete rods [29,43]. Slower rate of precipitation and absence of shear flow are possible factors for reduced particle aggregation under static conditions. The particles attach to each other to form fibers or sheets depending on the synthesis conditions [44]. Varying the HCl concentration is a way to control the length and agglomeration of the rods [45,46].

2.1.2 HMM

Hiroshima mesoporous material (HMM) is a silica material consisting of small spherical particles with non-ordered mesopores [38]. A cationic surfactant, cetyltrimethylammonium bromide (CTAB) (Figure 5), is used as the structure directing agent, TEOS as silica source, and octane and styrene as hydrophobic components. An oil-in-water emulsion is formed with styrene, octane and TEOS constituting the oil phase. Hydrolysis and condensation of TEOS into silica and polymerization of styrene into polystyrene are taking place simultaneously inside the drops.

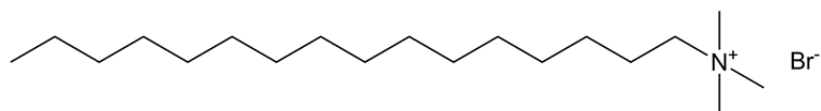


Figure 5. The cationic surfactant cetyltrimethylammonium bromide, CTAB.

A basic amino acid is used as catalyst for the silica condensation and also functions to limit the particle growth. The amino acid covers the nanoparticles during the growth process, thus preventing agglomeration. This mechanism is proposed to be due to the electrostatic interaction between anionic silicates ($\equiv\text{SiO}^-$) and protonated amino groups on the amino acid in combination with hydrogen bonding between amino acid molecules [30]. The organic materials, i.e., polystyrene, octane and the amino acid, are removed by heat treatment, yielding small silica particles with mesoporous structure. Figure 6 shows a schematic of the synthesis process.

The particle diameter can be controlled by varying the amount of octane in the reaction mixture. An increased amount of the hydrocarbon generates larger particles. It is also possible to tune the pore size by varying the amount of styrene. A larger amount of styrene results in an increase in polystyrene formation, hence larger pores.

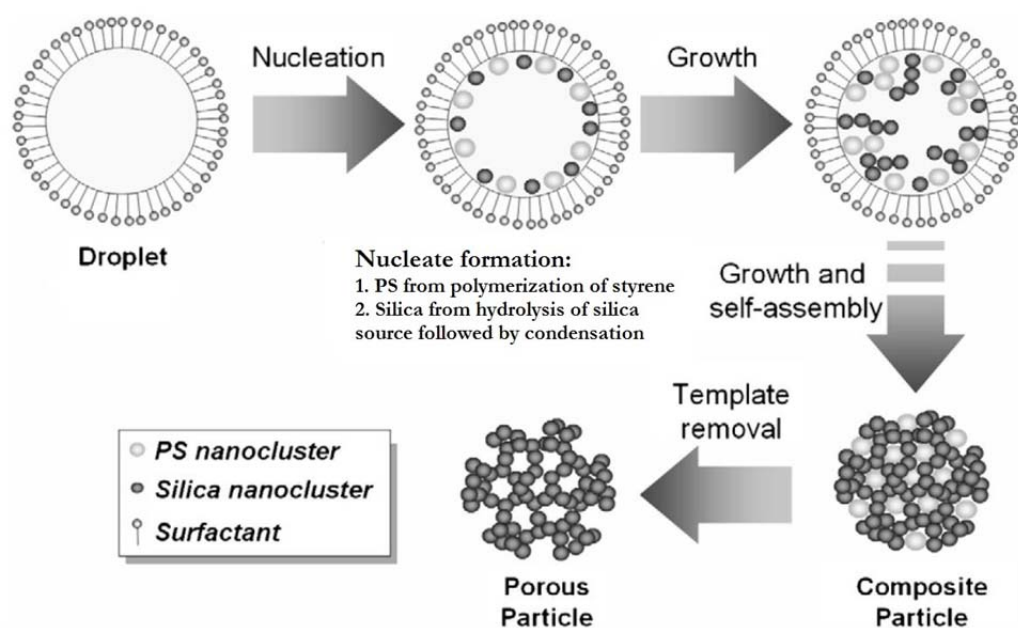


Figure 6. Proposed synthesis route of HMM. Redrawn from Nandiyanto et al [38].

Chapter 3

IMMOBILIZATION OF ENZYMES

The use of enzymes as biocatalysts in industry is a field that is attracting considerable interest. Enzymes have a high stereo- and regioselectivity and a high catalytic efficiency under mild reaction conditions. These qualities make them an environmentally friendly alternative to conventional synthetic catalysts. Synthetic catalysts often demand harsh chemical conditions and multi-step processes, leading to excessive energy consumption and generation of much waste. Examples of applications for which enzymes have been and are being developed are in the manufacture of food (e.g. bread, cheese, butter, beer), fine chemicals (e.g. vitamins, amino acids), and pharmaceuticals [47]. They are also used in detergent formulations and for analytical and diagnostic purposes [47,48]. However, enzymes have in general a quite low long-term operational stability and are difficult to recover from the reaction media, making the reuse very limited. A strategy to overcome these limitations is to immobilize the enzymes. There are numerous methods of immobilization, including binding of the enzymes on a solid support or carrier, enzyme entrapment inside a material and cross-linking of enzymes to each other [6,9,10,49].

3.1 Use of mesoporous silica for enzyme immobilization

Mesoporous silica is a widely studied material and has several advantages as a support for enzymes. As mentioned in Chapter 2, they have a large surface area and well-ordered and uniform pores with an adjustable pore size in a range suitable for biomolecules, like enzymes. Moreover, the surface can be easily functionalized. The porous structure enables a large quantity of enzyme to be immobilized compared to a flat surface. Entrapment in the pores may also protect the enzymes from the surrounding media. The enzymes can be immobilized to the porous material either by covalent binding, physical adsorption or electrostatic attraction. Figure 7 shows an illustration of an enzyme immobilized in the pores of hexagonally ordered mesoporous silica.

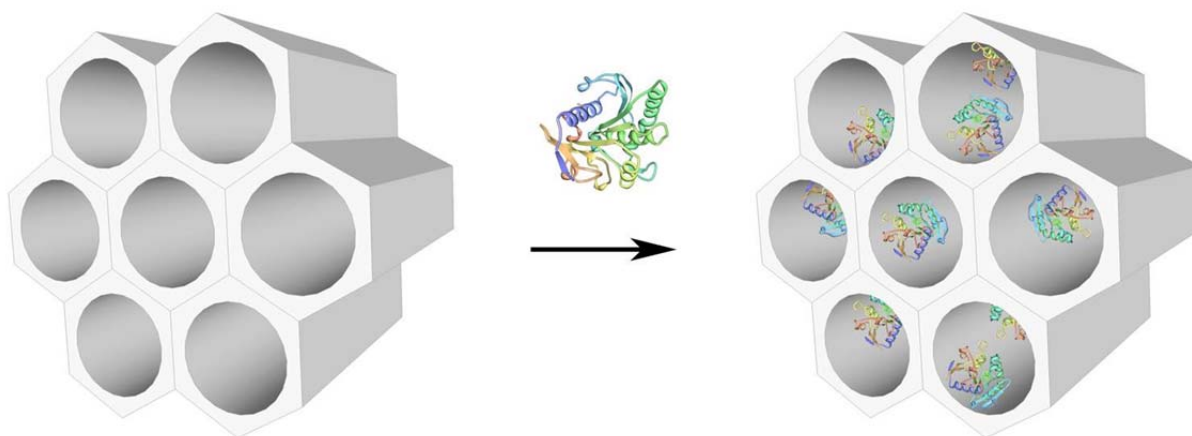


Figure 7. Enzymes immobilized into the pores of hexagonally ordered mesoporous silica.

3.1.1 Immobilization methods

Covalent immobilization involves binding of reactive groups on the enzymes to a chemically active surface (Figure 8a). The reactive groups may for example be amino, thiol or hydroxyl groups on amino acid side chains located on the enzyme surface. Amino groups in the side chain of lysine or other dibasic amino acids are usually the preferred groups because of their abundance. Thiol groups are very potent but are generally involved in disulfide bridges that affect the protein conformation [7]. The silica surface is activated by functionalizing the silanol groups. One typical procedure to covalently bind the enzyme to silica is to first functionalize the silica surface with a silane coupling agent containing an amino group, for example aminopropyltriethoxy silane (APTES), then add a cross-linking agent, for example glutaraldehyde. Glutaraldehyde binds covalently to the amine functionalized silica surface. Finally, the enzyme is added and glutaraldehyde also forms covalent bonds with amino groups on the enzyme surface [50] (Figure 9). Thus, glutaraldehyde acts as a linker between the enzyme and the APTES-modified silica surface. Covalent binding of the enzyme to the silica carrier provides stable enzymes that can withstand elevated reaction temperatures and can be reused without leaking out from the carrier. The major drawback is reduced enzymatic activity due to conformational changes upon attachment. If the covalent bond is involved in or close to any essential part of the catalytic site, the activity may be completely lost. Covalent bonds between enzyme and silica may also contribute to clogging of the pore openings, thus preventing enzymes from reaching the interior of the pores.

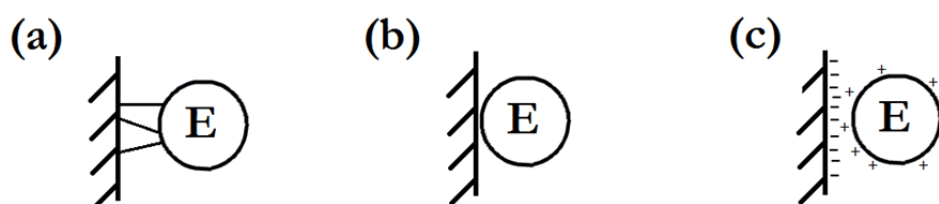


Figure 8. Methods of enzyme immobilization to mesoporous silica. (a) Covalent bonding, (b) physical adsorption, (c) electrostatic interaction.

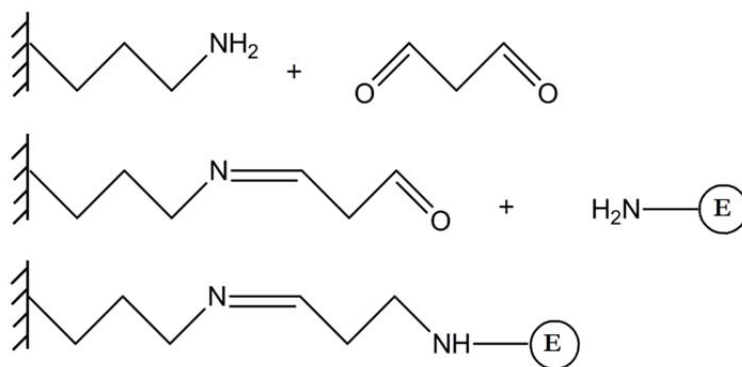


Figure 9. Covalent binding of an enzyme to silica functionalized with APTES. Glutaraldehyde ($\text{O}=\text{CH}-\text{CH}_2-\text{CH}=\text{O}$) is used as linking agent

Physical adsorption is the most simple immobilization method and therefore also frequently used in large-scale production (Figure 8b). The method involves only weak interactions such as hydrogen bonding, acid-base interactions and van der Waals attraction. The advantages are that no activation of the support is needed and that the risk of enzyme denaturation due to strong binding is minimized. A limitation with this method is that the interactions often are too weak to prevent the enzyme from leaking out of the material. To minimize the leaking it is important to tailor-make the material regarding pore size etc. and to find the optimal conditions for the specific enzyme. Ionic strength of the solution, pH and temperature are parameters that generally affect the enzyme adsorption.

The adsorption of enzymes to the silica surface can be improved and the leaking can be minimized if there are electrostatic interactions between oppositely charged residues on the enzyme molecules and the silica surface (Figure 8c). The overall charge on the enzyme surface and silica surface can be controlled by varying the pH of the solution. An attractive interaction between enzyme and silica is obtained at a pH somewhere in-between the point of zero charge (pzc) of silica (pzc ~ 2) and the isoelectric point (pI) of the specific enzyme [23]. The isoelectric point (pI) is the pH where a surface or a molecule has no net charge. At a pH below the pzc of silica or above the pI of the enzyme the two components will have the same net charge, which will lead to repulsive electrostatic forces. However, as is discussed in Paper II, the enzymes are flexible and may adopt a conformation in the vicinity of a support surface such that they experience attractive electrostatic interactions even if their net charge is the same as that of the support. It is, for instance, known that enzymes adsorb readily at negatively charged surfaces also well above their pI [51,52].

Adsorption through electrostatic interactions is a milder method compared to covalent binding so the degree of conformational changes and activity loss is generally lower. The immobilization procedure is also less complex and is therefore more suitable for large scale preparations.

3.1.2 Support properties

Enzymes can vary radically in size, shape, isoelectric point, surface charge, charge distribution, catalytic performance, etc. During enzyme immobilization it is important to keep this in mind and to adapt the physicochemical properties of the mesoporous material to the particular enzyme properties. In addition to the immobilization methods discussed in Section 3.1.1, the support properties like pore size, particle size and particle morphology are crucial factors to consider. Both enzyme loading and catalytic performance inside the support can be significantly improved with an optimized support [23,53,54].

The size of the pore opening in relation to the enzyme determines whether the enzyme will fit inside the pores or not. Enzymes that are larger than the pore openings will obviously not fit inside the pore at all but may instead adsorb on the outer surface of the particles [24]. If the pores and the enzyme are of similar size, or if the pores are slightly larger, the enzyme can diffuse into the pores and will be protected from the surroundings [55,56]. However, the diffusion into the narrow pores may be slow. Enzymes can also get stuck in the pore openings and the loading may therefore not be optimal. The diffusion of substrate to the active site can also be hindered if the pores are too narrow [57]. On the other hand, if the pore openings are much larger than the enzyme, a high loading can be obtained. Instead, leaking may be an issue and the enzymes will not be as protected from the surrounding media as if the pores are of matching size [55,57]. The enzyme stability also influences the optimal pore size. An unstable enzyme may need a narrower pore size compared to a relatively stable enzyme. A confining effect in a narrow pore can also enhance the specific activity due to a beneficial conformational change of the enzyme [58].

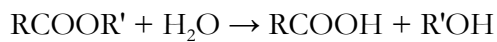
The size of the mesoporous silica particles can also affect the both the enzyme loading and the catalytic activity. Smaller particles but with the same overall pore volume can improve the loading since shorter pores will decrease the diffusion distance and minimize empty space far down the pores [54]. The substrate will then be able to reach a larger relative amount of active sites within a certain time.

3.2 Enzymes

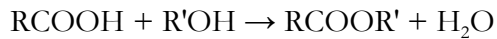
3.2.1 Lipase

Lipases (triacylglycerol acylhydrolases, E.C. 3.1.1.3) are a group of water-soluble enzymes that are the key enzymes in metabolism and fat digestion. They are recognized as one of the most important group of enzymes in biotechnology, with applications in food, detergent, pharmaceutical, leather, textile, cosmetic and paper industries [59]. Lipases are a sub group of esterases and are also called serine hydrolases. They catalyze the hydrolysis of triacylglycerol to glycerol and free fatty acids in aqueous media. In organic media they catalyze the reverse reaction, where esters are synthesized and transesterified.

Hydrolysis

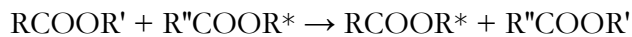


Esterification

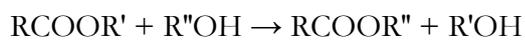


Transesterification

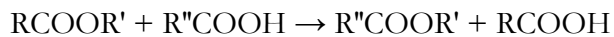
Interesterification



Alcoholysis



Acidolysis



In contrast to conventional esterases, lipases are surface active and the enzymatic activity is often greatly increased when the lipase is close to an interface. This behavior is due to the unique structural characteristics of lipases. The active site is covered with a hydrophobic α -helical unit, called the “lid” that changes its conformation to an open state when interacting with an interface [60]. Thus, the active site is revealed. Immobilizing lipases on interfaces can therefore be very useful. The active site in lipases holds a catalytic triad, i.e., the three amino acids directly involved in the catalytic process. The triad is composed of serine, histidine, and aspartate or glutamate. A similar triad is found in serine proteases. Close to the triad is an oxyanion hole that stabilizes the carbonyl group of the substrate during the hydrolysis. In Paper I lipase from *Mucor miebei* (MML) is studied (Figure 10a). The pI of MML is 3.8, the molecular weight is 32 kDa, and the hydrodynamic diameter is 4.5 nm [61]. In Paper II lipase from *Mucor miebei* is compared with lipase from *Rhizopus oryzae* (ROL) that has the same size (32 kDa) but a different pI (7.6) [62].

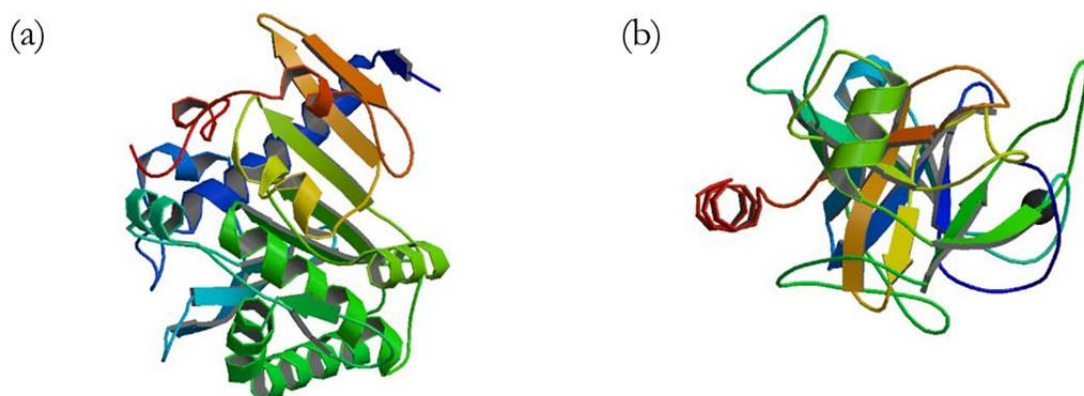


Figure 10. Structure of (a) lipase from *Mucor miebei* and (b) trypsin from *bovine pancreas*.

3.2.2 Trypsin

Trypsin (E.C. 3.4.21.4) is, like lipase, an important enzyme in the metabolic process where it degrades proteins. It is an enzyme with many applications in for example food, detergents, and waste management, as well as in the diagnostics and pharmaceutical industries [63]. More specifically, trypsin is a serine protease, also called peptidase that catalyzes the hydrolysis of peptide bonds at the carboxyl side of the amino acids lysine and arginine. As mentioned in Section 3.2.1 the active site contains a catalytic triad and an oxyanion hole that stabilizes the intermediate molecule during the process. The triad consists of a serine, a histidine and an arginine, where serine acts as the nucleophilic amino acid towards positively charged amino acids [64]. Since trypsin is a protease it can also degrade adjacent trypsin molecules (autolysis) as well as other enzymes in a solution. This is obviously an extensive problem and the stability of a trypsin solution is therefore very low in many industrial processes. Such degradation can to a large extent be overcome by immobilization because the trypsin molecules will then be prevented from reaching each other.

In Paper I trypsin from *bovine pancreas* (BPT) (Figure 10b) is compared with lipase from *Mucor miehei*. The pI of this trypsin is 10.5, the molecular weight is 23 kDa, and the hydrodynamic diameter is 3.8 nm [24].

3.2.3 Feruloyl esterases

Feruloyl esterases (FAEs) (E.C. 3.1.1.73) are commonly found in fungi and participate in the cell wall degradation of plants. They are a subclass of carboxylic ester hydrolases that catalyze the hydrolysis of ester bonds between hemicelluloses and lignin, releasing hydroxycinnamic acids and sugars (polysaccharides) [65,66]. Figure 11 shows the structure of ferulic acid (FA), 4-hydroxy-3-methoxycinnamic acid, which is an important hydroxycinnamic acid derivative.

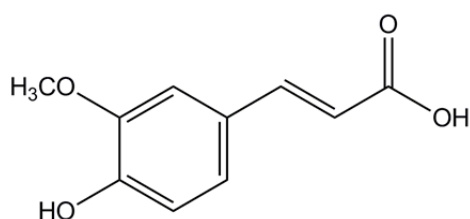


Figure 11. Ferulic acid.

Possible applications for FAEs are numerous, including pulp and paper industry, production of fuel ethanol and farming industry [66]. Hydroxycinnamic acid derivatives have been shown to have both antioxidant and antitumor properties [67,68]. It is therefore of great interest to add these compounds to foods, cosmetics and therapeutics. However, it is often desirable to modify the properties of the hydroxycinnamic acids. For example, their hydrophobicity must be increased for use in oil-based products. Under certain conditions FAEs have been shown to catalyze the reverse reaction and can be used in the esterification of hydroxycinnamic acids.

Previous studies have shown that it is possible to promote the reverse reaction (esterification and transesterification) by confining the FAEs in the oil droplets of oil-in-water microemulsions [69]. This may be due to a change of the FAE into a more favorable conformation, as well as a change in substrate access.

In Paper III the immobilization of FAE into mesoporous silica is studied and how the activity is affected by confining the enzymes into silica nanopores.

Chapter 4

ANALYTICAL TECHNIQUES

Characterization of mesoporous materials demands a combination of analytical techniques. Transmission electron microscopy (TEM), scanning electron microscopy (SEM), physisorption and small angle X-ray scattering (SAXS) are all used to determine the particle morphology, pore structure, pore size and pore size distribution, specific surface area and pore volume of the materials prepared in this work. The activity of the enzymes immobilized in the various materials and the enzyme concentrations are evaluated with UV/Vis spectrometry.

4.1 Transmission electron microscopy

Transmission electron microscopy (TEM) is a high resolution microscope technique that utilizes electrons to visualize specimens with a magnification up to 10^6 . Due to the short wavelength of electrons it is possible to obtain a resolution in the range of 1 \AA . An electron beam is accelerated in vacuum at high voltages through a thin sample. The image is obtained by focusing the transmitted electrons onto a fluorescent screen. Thicker regions in the sample scatter more electrons compared to thinner regions. Therefore, thicker regions with high scattering will appear darker on the screen than thinner regions.

In this thesis, a JEM-1200 EX II TEM (Jeol, Tokyo, Japan) operated at 120 kV was used for determining the local pore structure and order of mesoporous silica and also for estimating the size of small silica particles. Thin specimens were prepared by grinding silica particles followed by dispersion in ethanol and sonication for 10 minutes. Complementary techniques were needed to confirm the results since TEM only displays a limited part of the sample.

4.2 Scanning electron microscopy

Scanning electron microscopy (SEM) is like TEM a non-destructive electron microscopy technique. An electron beam is scanned over the specimen creating signals when the electrons interact with the sample. Secondary electrons and backscattered electrons emitted from the surface are detected and utilized to visualize a three-dimensional topology, surface morphology and surface composition of materials with a resolution in the nm range.

In this work, a Leo Ultra 55 FEG SEM (Leo Electron Microscopy, Cambridge, UK) was used to study the particle size and morphology of the mesoporous silica materials and also to some extent the mesoporous structure. For insulators, like silica, it is common to coat the surface with a metal in order to prevent charging of the material. However, the metal coating aggravates a detailed observation of the pore structure. By instead using a low accelerating voltage (2.0 kV) the surface charging can be minimized. Prior to use, silica particles were dispersed in ethanol and sonicated for 10 minutes. The secondary electrons were collected with an in-lens detector.

4.3 Physisorption

Physisorption is a method to characterize the specific surface area, pore volume, pore size and pore size distribution of solid porous materials. The method utilizes attraction between gas molecules and the atoms on the surface of the porous material. The most common gas in this technique is nitrogen, but krypton and argon are also used for characterizing materials with small surface areas. The sample is first degassed in a vacuum oven to remove any adsorbed contaminants followed by cooling to 77 K and then exposure of nitrogen gas under controlled pressures. The surface area is quantified by creating a monolayer of nitrogen molecules at the solid surface with an increasing pressure. Using the universal gas law and the Brunauer-Emmett-Teller (BET) gas adsorption method [70] the adsorbed amount can be calculated. Information about the pore volume, pore size and shape of the pores is obtained by further saturating the pores with nitrogen gas. The partial pressure (p/p_0), is stepwise increased until the point of condensation is reached followed by a pressure reduction resulting in gas evaporation. Pore size calculation is performed with the Barrett-Joyner-Halenda method [71].

The data is presented as adsorption/desorption isotherms which can be grouped into six types (I-VI), shown in Figure 12. Typical for a mesoporous material is a well-defined hysteresis loop (type IV), due to the capillary condensation inside the mesopores. The first part of the curve represents the monolayer condensation where point B indicates a complete monolayer. There are four types of hysteresis loops (H1-H4), shown in Figure 13, where the shape depends on the type of pore structure. Mesoporous materials with a uniform pore structure and narrow pore size distribution typically result in adsorption and desorption isotherms almost vertical and parallel to each other (H1). A H2 loop indicates occurrence of non-uniform pores whereas slit-shaped pores often result in a H3 loop. Slit-shaped pores are also associated with a H4 loop but the almost horizontal plateau indicates microporosity.

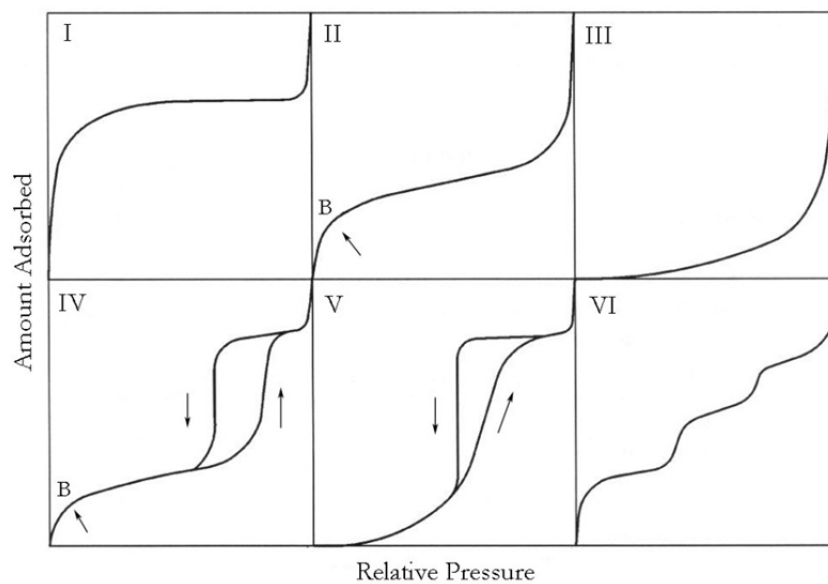


Figure 12. Types of physisorption isotherms according to IUPAC classification [72].

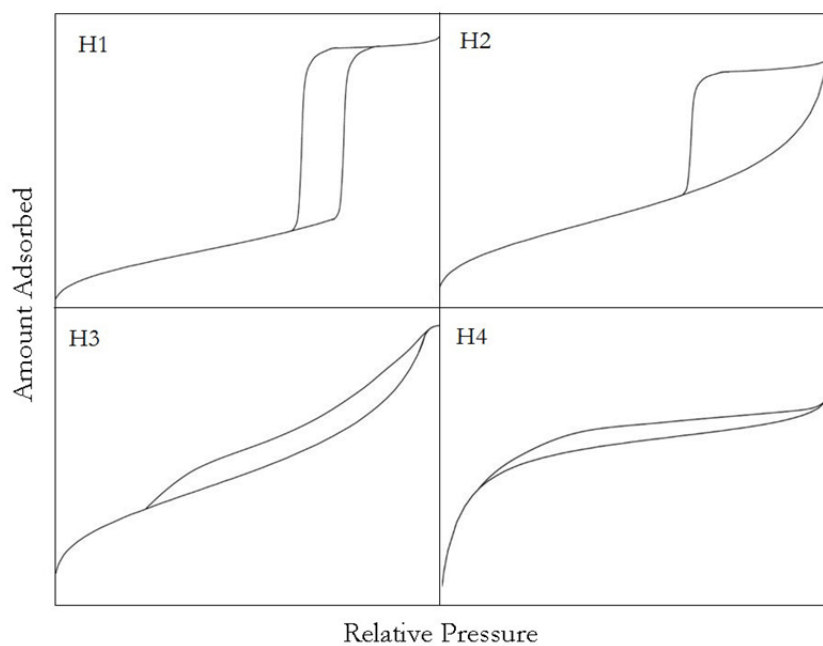


Figure 13. Types of hysteresis loops according to IUPAC classification [72].

In this thesis, mesoporous silica particles were analyzed in a Micromeritics ASAP 2010 instrument after degassing the samples in a vacuum oven at 225 °C for 2 h.

4.4 Small angle X-ray scattering

Small angle X-ray scattering (SAXS) is a method that utilizes the short wavelength of X-rays for analyzing the intermolecular structure of ordered materials. The incoming X-rays are of the same order of magnitude as the distance between the lattice planes in a crystalline material. Scattered radiation, due to interference with the electron clouds around the atoms in the material, is detected and the intensity is plotted as a function of the scattering angle (2θ). The regular pattern in a crystal gives rise to peaks in the plot due to constructively interfering scattered radiation characteristic for a specific crystal structure. The distance between the peaks represents spacing of the crystal planes that can be calculated using Bragg's law:

$$n\lambda = 2d_{hkl} \sin \theta \quad (2)$$

where n is an integer, λ the wavelength of the incoming beam, d_{hkl} the spacing between the parallel crystal planes and θ the angle between the incoming beam and the crystal plane (Figure 14). The indices h , k , and l , denote a crystal plane orthogonal to a direction, where $l = 0$ for hexagonal structures (cylindrical assemblies crystallized in a two dimensional hexagonal lattice).

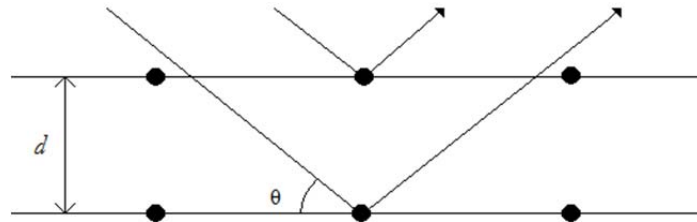


Figure 14. Illustration of X-ray diffraction according to Bragg's law.

The structure can be determined from the relative distance between the Bragg peaks, denoted q_{hk} . The spacing is defined as

$$d_{hk} = \left[\frac{4}{3a^2} (h^2 + k^2 + hk) \right]^{-1/2} \quad (3)$$

and

$$q_{hk} = \frac{2\pi}{d_{hk}} = \frac{4\pi}{\sqrt{3}a} \sqrt{h^2 + k^2 + hk} \quad (4)$$

where a is a unit cell length (the distance between the centers of adjacent cylinders). According to equation 4 the relative distance between the Bragg peaks for a hexagonal structure are $q_{10}:q_{11}:q_{20}:q_{21}:q_{30}:q_{22} = 1:\sqrt{3}:2:\sqrt{7}:3:\sqrt{12}$. Also typical for mesoporous silica with hexagonally structured pores are 2θ angles below 3° . A typical plot for a hexagonal pattern is shown in Figure 15.

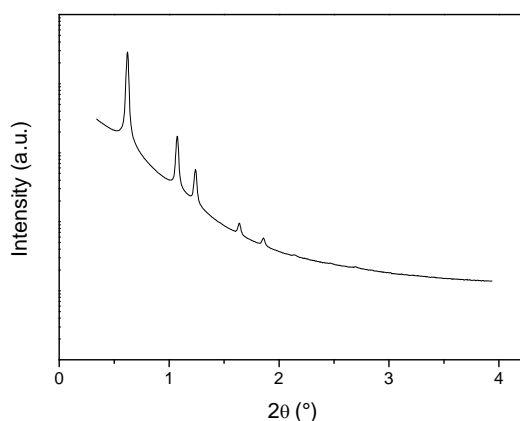


Figure 15. Typical SAXS spectrum for a hexagonally ordered material.

Atoms with high electron density, like silica, scatter X-rays with a relatively high intensity, but the intensity can be further increased by using a synchrotron with a high flux of radiation. The photons emitted by electrons circulating in a magnetic field are used to irradiate the sample. In this work SAXS measurements were performed on the I711 and I911 beam lines at the MAX-lab synchrotron facility (Lund, Sweden).

4.5 UV/Vis spectrometry

UV/Vis spectrometry is an analytical tool for quantitative determination of analytes. It is based on measurement of the absorbance in the ultraviolet and visible spectral region when a beam of parallel radiation passes through a solution of a compound. Electromagnetic energy from the beam is transferred to the atoms or molecules in the sample solution. This absorption of energy causes excitation of the electrons to a higher energy state if the excited photons, with a specific wavelength, exactly match the energy difference between the ground state and one of the excited states of the compound. The electrons in a molecule are bound in a specific way, and therefore all compounds have a unique absorption spectrum. The amount of light absorbed is directly proportional to the path length through the solution and the concentration of the absorbing species is expressed by the Lambert-Beer law:

$$A = \log(I_0/I) = \epsilon cl \quad (5)$$

where A is the absorbance or extinction, I_0 and I the intensities of the monochromatic light before and after passing through the sample, ϵ the molar absorptivity or extinction coefficient, c the concentration of the compound and l the path length. The molar absorptivity is a substance-specific constant, describing the light absorbing ability at a given wavelength under specified conditions regarding solvent, pH, temperature, etc. From this relation the concentration can be plotted as a linear function of the absorbance. UV/Vis absorption spectroscopy is normally sensitive to electrons participating in the formation of multiple bonds or aromatic groups within organic molecules.

4.5.1 Enzyme activity

In this study the activity of lipase and trypsin were estimated by measuring the formation of two organic compounds. The activity of lipase was assayed by monitoring the catalytic hydrolysis of 4-nitrophenyl acetate (pNPA) into 4-nitrophenol (pNP) and acetic acid (Figure 16). Under alkaline conditions pNP is deprotonated to 4-nitrophenolate, which is bright yellow. The absorbance is detected at 400 nm ($\epsilon_{\text{molar}} = 14,200 \text{ M}^{-1} \text{ cm}^{-1}$).

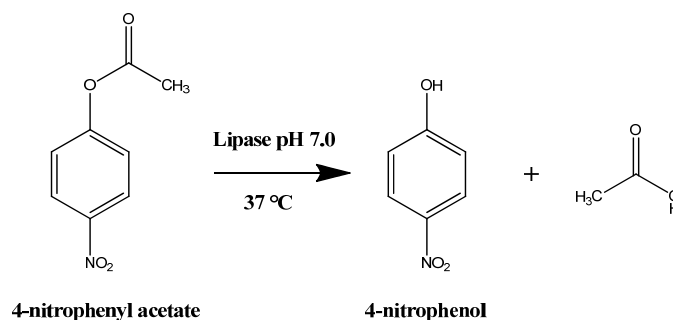


Figure 16. Lipase-catalyzed hydrolysis of 4-nitrophenyl acetate (pNPA).

The activity of trypsin was estimated by monitoring the catalytic hydrolysis of N- α -benzoyl-DL-arginine-4-nitroanilide (BAPNA) into 4-nitroaniline (Figure 17). The absorbance can be detected at 405 nm ($\epsilon_{\text{molar}} = 10,500 \text{ M}^{-1} \text{ cm}^{-1}$). The measurements were carried out using a Agilent HP8453 spectrophotometer.

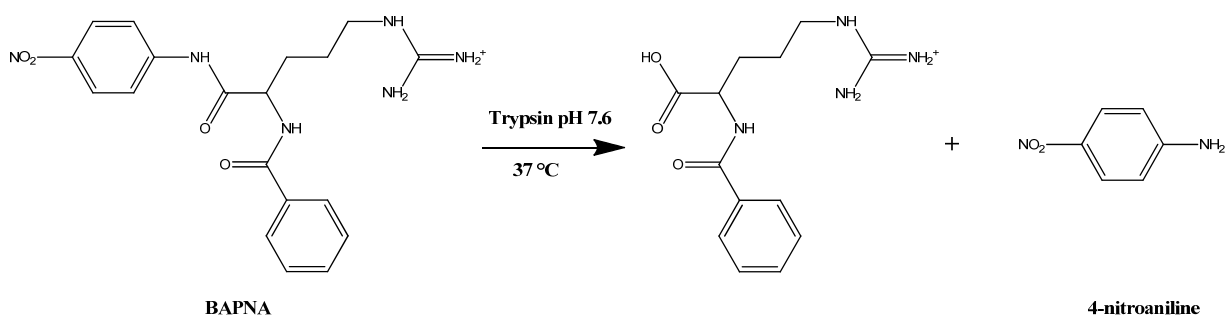


Figure 17. Trypsin-catalyzed hydrolysis of N- α -benzoyl-DL-arginine-4-nitroanilide (BAPNA).

4.5.2 Protein concentration

Ultraviolet light absorption

UV/Vis spectrometry is a widely used method for concentration measurements of proteins. Proteins have characteristic absorption peaks at 200 nm and 280 nm. All peptide bonds absorb UV light at 200 nm whereas the aromatic amino acids tryptophan and tyrosine absorb UV light at 280 nm. The absorbance at 200 nm is mainly due to the many peptide bonds in a protein. However, many other substances also absorb light in this area and 200 nm is therefore not a suitable wavelength for estimating the concentration of proteins. Therefore measurements are normally performed at 280 nm. This spectrophotometric method, used in Paper II, is straightforward and rapid and demands no preparation of the samples. But one should be aware

of the possible interference by contaminating nucleic acids (and possibly other substances) that absorb strongly at 260 nm.

Colorimetric assays

Colorimetric assays are also used for determination of protein concentration. Well-known examples are the Lowry assay [73], the BCA assay [74] and the Bradford assay [75]. These assays are all based on a color shift of an extrinsic molecule in the presence of a protein. The BCA assay has been used in Paper I and is based on reduction of Cu^{2+} to Cu^+ by proteins under alkaline conditions followed by detection of the generated Cu^+ with a reagent containing bicinchoninic acid (BCA) (Figure 18). The cuprous ion chelates two BCA molecules and the complex absorbs visible light at 562 nm. According to Wiechelman et al. the reduction of copper is performed by the aromatic amino acid residues in cysteine, cystine, tryptophan and tyrosine together with peptide bonds [76].

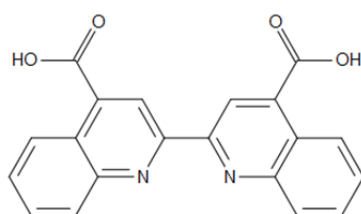


Figure 18. Bicinchoninic acid.

In the Bradford assay, used in Paper III, the binding of the dye Coomassie brilliant blue G-250 (CB) (Figure 19) to proteins is utilized for determining protein concentration. The dye is converted from a red form to blue upon protein binding in acidic conditions. The mechanism is not fully understood but CB probably binds mainly to the charged amino acids residues arginine and lysine. The protein bound dye has an absorption maximum at 595 nm.

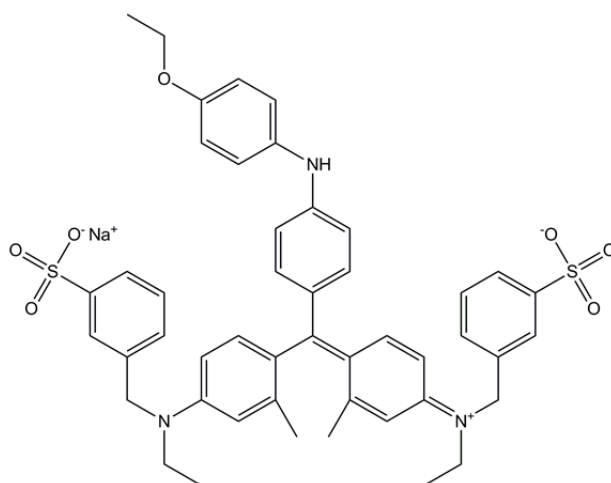


Figure 19. Coomassie brilliant blue G-250.

4.6 Optical tensiometry

Surface tension of a liquid can be measured with pendant drop shape analysis using an optical tensiometer [77,78]. A drop of the liquid is hanging from a syringe tip and the shape of the drop is determined by the balance between surface forces and gravity. The surface tension is determined by fitting the shape of the drop to the Young-Laplace equation, which relates interfacial tension to drop shape:

$$\Delta P = \gamma(1/R_1 + 1/R_2) \quad (6)$$

where ΔP is the interfacial pressure difference, γ the interfacial tension, and R_1 and R_2 are the radii of the drop (see Figure 20).

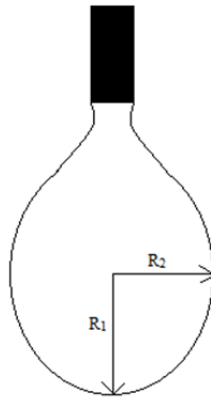


Figure 20. A pendant drop.

Surface tension measurements of lipase solutions are described in Paper II using an optical tensiometer, Attension, Theta Lite, KSV Instruments for pendant drop shape analysis.

Chapter 5

RESULTS AND DISCUSSION

In this thesis mesoporous silica particles have been synthesized and used as support for biocatalysts. Different approaches have been utilized to obtain silica material with varying pore size, particle size and particle morphology. The work was focused on investigating how varying properties of the mesoporous silica influence the loading capacity and the catalytic performance of different hydrolytic enzymes.

5.1 Characterization of mesoporous silica

The morphological and structural characterization of the mesoporous silica particles was performed by the combined use of SEM, TEM, nitrogen physisorption and SAXS. Particles with four different sizes and morphologies were synthesized using different approaches. See attached papers for detailed descriptions of the preparation methods. In Paper I and Paper III a conventional synthesis of SBA-15 resulted in silica particles with rod-like shape, about 2 μm in length and 1 μm in diameter (Figure 21a). The particles were agglomerated into clusters. The addition of a potassium salt to the reaction mixture together with the use of static conditions during the condensation resulted in particles with a different type of morphology (Figure 21b) (Paper II). The particles were broader and shorter and also less agglomerated compared to the conventional SBA-15 particles. As discussed in Section 2.1.1, some inorganic salts of polyvalent anions can enhance the interaction between silica species and the polyoxyethylene segments of the nonionic block copolymer, thereby affecting the morphology of the silica particles. The particle agglomeration was reduced by decreasing the stirring time during the silica condensation step. The size of the particles obtained by the modified SBA-15 synthesis was around 1000 nm (MPS-1000). By using a low temperature synthesis with addition of heptane and NH_4F to the conventional synthesis, smaller particles, about 300 nm (MPS-300) with a rod-shaped morphology, were obtained (Figure 21c) (Paper II). A decrease in stirring time and increase in HCl concentration yielded discrete non-agglomerated particles [45]. The very small particles (Figure 21d) described in Paper II were synthesized by forming an oil-in-water emulsion using a cationic surfactant and with styrene, the silica precursor and octane constituting the oil phase (described in Section 2.1.2). A composite material with silica and polystyrene clusters were formed inside the dispersed phase. Spherical mesoporous silica particles around 40 nm in diameter (MPS-40) were obtained after removal of the organic components by calcination.

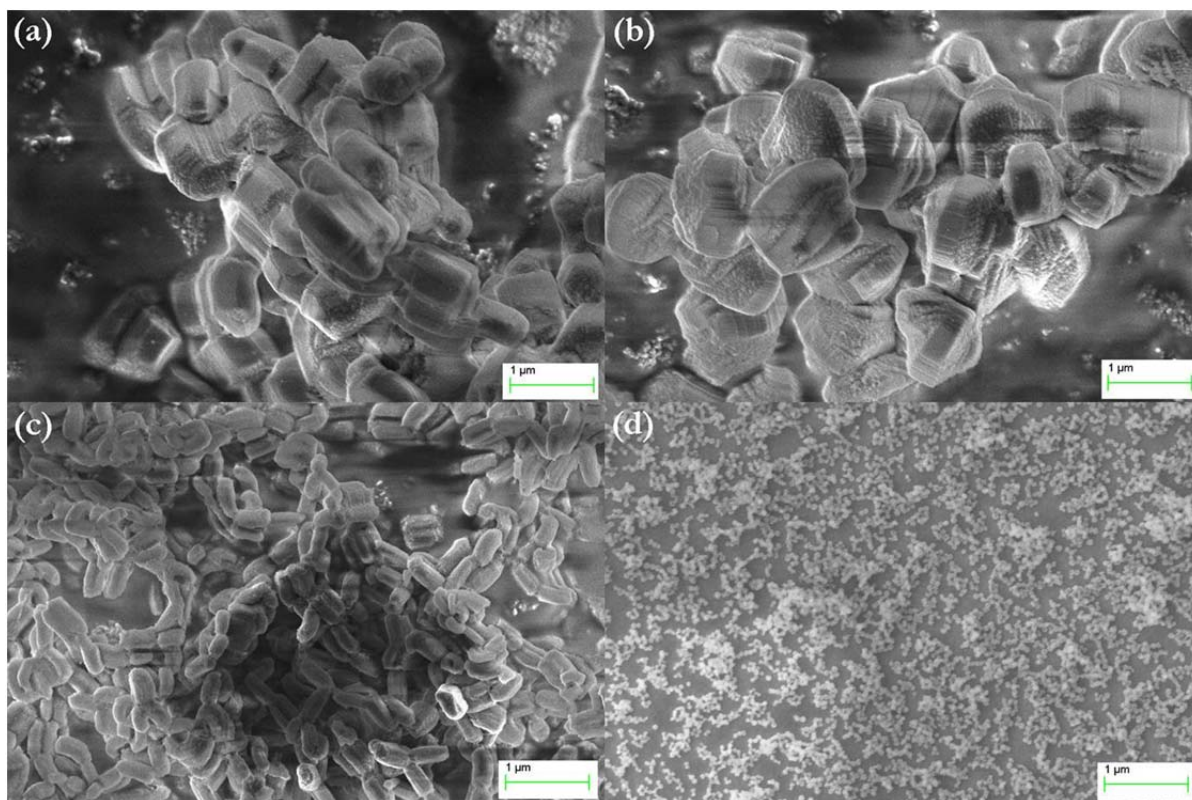


Figure 21. SEM micrographs of the mesoporous silica particles. (a) SBA-15, (b) MPS-1000, (c) MPS-300, and (d) MPS-40.

Typical TEM micrographs of calcined SBA-15, MPS-1000 and MPS-300, shown in Figures 22a and 22b, displayed hexagonal patterns with long range order and uniform pores. The TEM micrographs of MPS-40 (Figures 22c and 22d), showed quite monodisperse particles but with non-ordered pore structure. Instead of cylindrical uniform pores, as for the SBA-15 materials, the pores were slit-shaped and more varied with respect to both size and shape. A particle size around 40 nm was confirmed.

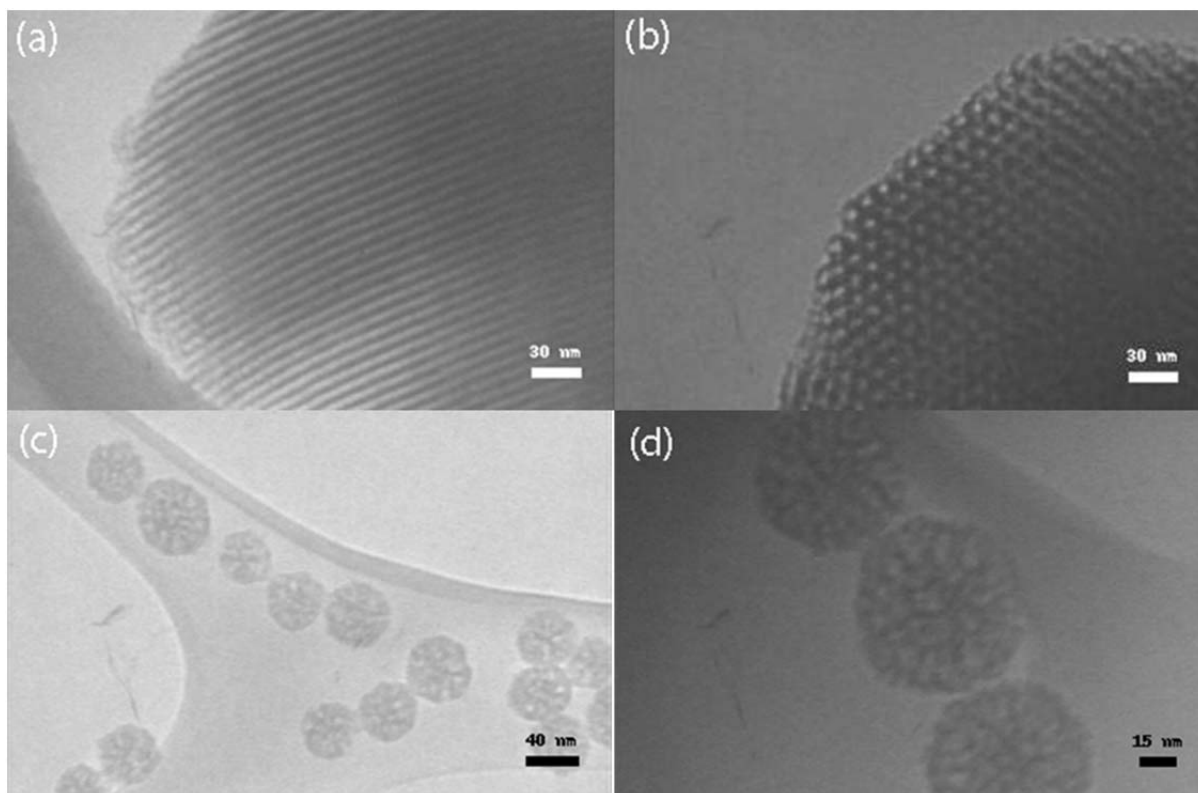


Figure 22. Representative TEM micrographs of the mesoporous silica particles. (a) and (b) SBA-15 (including MPS-1000 and MPS-300), (c) and (d) MPS-40.

N_2 -sorption isotherms of the calcined materials, shown in Figure 23a, confirm the pore structure observed in the TEM micrographs. SBA-15, MPS-1000 and MPS-300 all exhibit an adsorption-desorption isotherm type IV and H1 hysteresis, characteristic of SBA-15 materials with cylindrical and hexagonally ordered mesopores. MPS-40 also displays a type IV sorption isotherm, representative of a mesoporous material but with H3 hysteresis, which is characteristic of slit-shaped pores. SBA-15 of three different pore sizes in Paper I and two different pore sizes in Paper III were synthesized. The pore size was tuned by varying the hydrothermal temperature during the aging process. According to the BJH method the synthesis temperatures 80 °C, 100 °C and 140 °C resulted in mesoporous materials with 5 nm, 6 nm and 9 nm diameter pores, respectively (see Table 1). They are here denoted MPS-5P, MPS-6P and MPS-9P, according to their pore diameter. All materials showed isotherms characteristic of hexagonal structures (Figure 23b). The obtained pore sizes for MPS-1000, MPS-300 and MPS-40 were all around 9 nm (see Table 2).

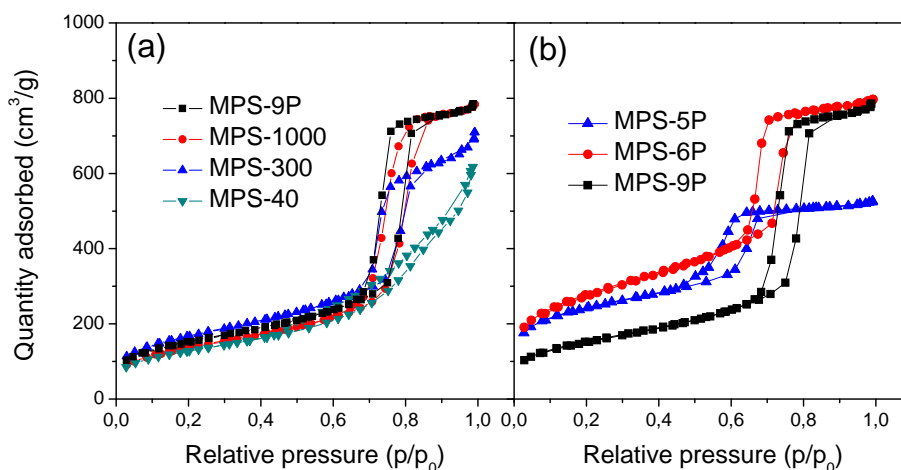


Figure 23. Nitrogen adsorption-desorption isotherms (a) MPS-9P, MPS-1000, MPS-300, and MPS-40 and (b) SBA-15 with three different pore sizes (MPS-5P, MPS-6P and MPS-9P).

Table 1. Material properties of SBA-15 with varied pore size, analyzed by nitrogen adsorption.

SBA-15	Denoted in papers	Synthesis temp. (°C)	BJH pore width (nm)	BET surface area (m ² /g)	Total pore volume (cm ³ /g)
MPS-5P	MPS-50 ¹	80	5.0	860	0.70
MPS-6P	MPS-60 ¹	100	6.0	986	1.08
MPS-9P	MPS-89 ¹	140	8.9	554	1.17
MPS-5P	MPS-5 ²	80	5.0	924	0.73
MPS-9P	MPS-9 ²	140	9.3	528	1.17

¹Paper I

²Paper III

Table 2. Material properties of mesoporous silica particles analyzed by nitrogen adsorption.

Material	BJH pore width (nm)	BET surface area (m ² /g)	Total pore volume (cm ³ /g)
MPS-1000	9.3	502	1.18
MPS-300	9.4	606	1.03
MPS-40	9.1	463	0.91

The pore size distribution of MPS-5P, MPS-6P and MPS-9P was narrow for all three pore sizes, independent of the hydrothermal temperature (Figure 24a). MPS-1000 and MPS-300 had similar pore size distribution as MPS-9P whereas the distribution was very wide for MPS-40 (Figure 24b). These results are in accordance with the TEM micrographs.

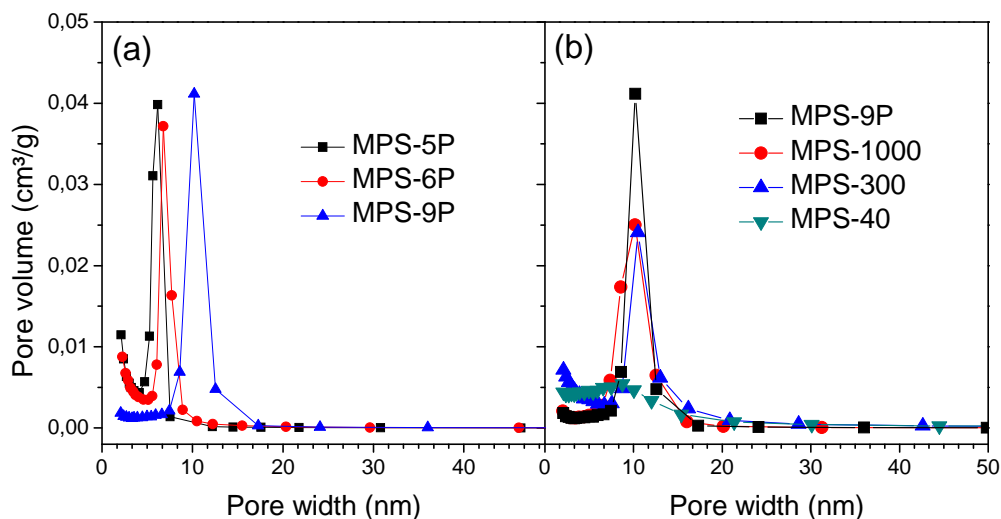


Figure 24. Pore size distribution of (a) SBA-15 with three different pore sizes (MPS-5P, MPS-6P and MPS-9P) and (b) MPS-9P, MPS-1000, MPS-300, and MPS-40.

Figure 25 shows the SAXS patterns of SBA-15 with varied pore size. At least three well-resolved peaks can be observed for all materials. These are indexed (100), (110) and (200), characteristic of a two dimensional hexagonal structure.

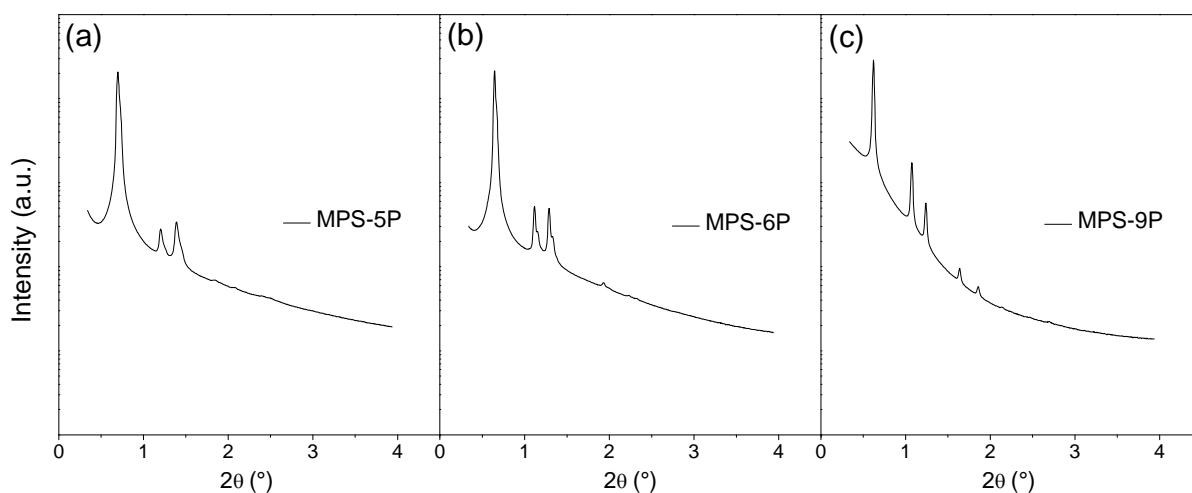


Figure 25. SAXS patterns of hexagonal mesoporous material with (a) 5 nm, (b) 6 nm, and (c) 9 nm pores.

The SAXS patterns of MPS-300 and MPS-40 are shown in Figures 26a and 26b, respectively. For MPS-300 three well-resolved peaks are observed, which can be indexed (100), (110) and (200). As expected, no pore order is observed for MPS-40.

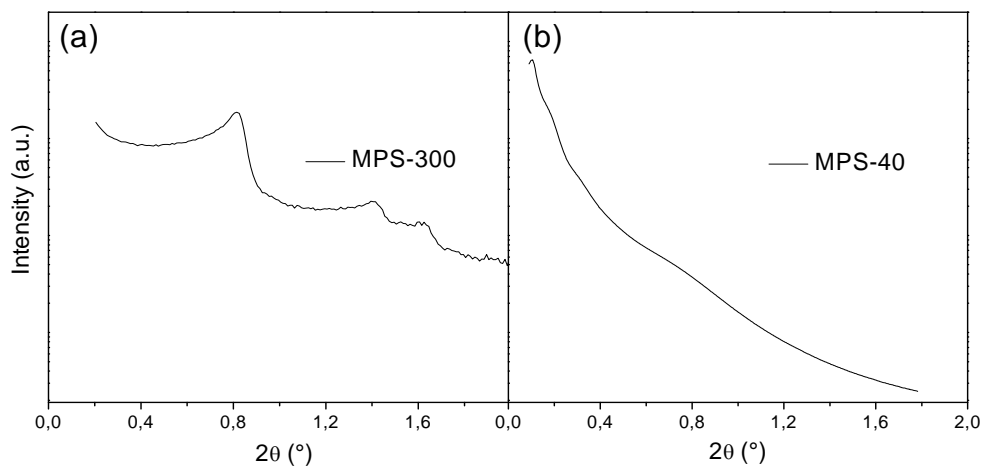


Figure 26. SAXS patterns of (a) MPS-300 and (b) MPS-40.

5.2 Immobilization of enzymes in mesoporous silica

5.2.1 Enzyme loading

In Papers I, II and III immobilization through physical adsorption of *bovine pancreatic* trypsin (BPT), *Mucor miehei* lipase (MML), *Rhizopus oryzae* lipase (ROL) and a crude enzyme preparation (Depol740L), shown to have feruloyl esterase (FAE) activity, were performed. In Papers I and III mesoporous silica with varied pore size was used as support. BPT and MML were compared in Paper I and FAE was studied in Paper III. The immobilization was followed over time to determine the time frame required to reach or get close to the loading equilibrium for each enzyme; i.e., the time at which no more protein is adsorbed. In Paper II mesoporous silica with varied particle size and morphology was used as support for MML and ROL. The physical properties of the enzymes are summarized in Table 3.

Table 3. Isoelectric point (pI), diameter (\varnothing), and molecular weight (M_w) of the enzymes.

Enzyme	pI	\varnothing (nm)	M_w (kDa)
BPT	10.5	3.8	23
MML	3.8	4.5	32
ROL	7.6	-	32
FAE	-	-	-

According to the BCA protein assay used in Paper I it took about one day for the BPT molecules to reach equilibrium when immobilized in MPS-5P, while almost all BPT was instantly incorporated into MPS-6P and MPS-9P (Figure 27a). It is important to note that some enzyme also adsorbs on the outer particle surface. The slow diffusion into MPS-5P indicates that the 5 nm pores are slightly too narrow for BPT, which has a diameter of 3.8 nm. The enzyme may get stuck in the pore entrances, subsequently blocking the pore. A fast immobilization rate is particularly important for proteases like trypsin since, as discussed in Section 3.2.2, they undergo autocatalytic degradation in solution. The immobilization of MML, which has a diameter of

around 4.5 nm, was very different from that of BPT, both in rate and in loading (Figure 27b). The loading capacity for MML inside the mesoporous silica particles clearly increased with increasing pore size but the immobilization rates were quite similar after the initial uptake. After two to three days the uptake levelled off. The final loading was found to be significantly lower than for BPT.

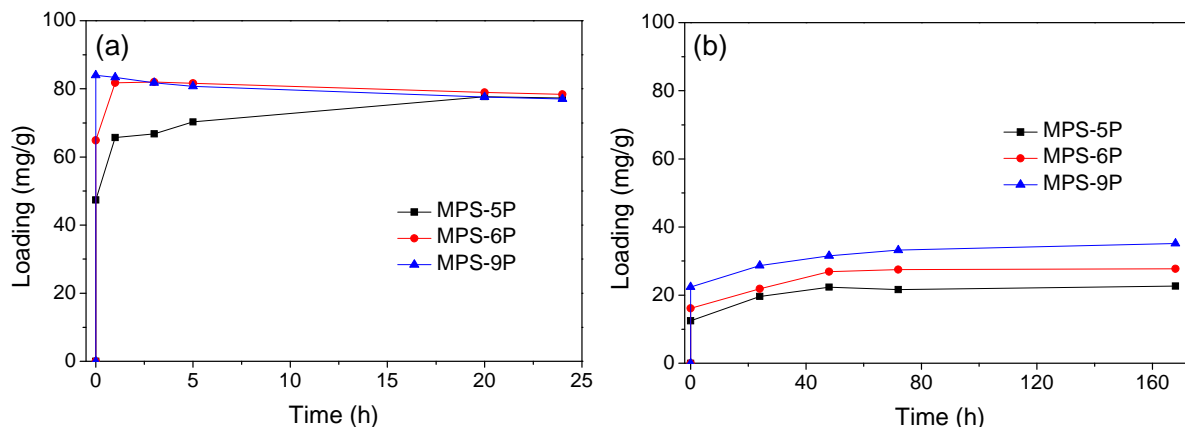


Figure 27. Immobilization rate of (a) BPT and (b) MML into SBA-15 with 5 nm, 6 nm and 9 nm pores in Tris-buffer of pH 7.6. The maximum loading amount is 96 mg enzyme per gram of silica support.

The difference between BPT and MML in immobilization capacity may be related to the fact that BPT is a smaller protein than MML. It may also be related to the difference in overall surface charge (Table 3). At pH 7.6 there will be attraction between the positively charged BPT and the negatively charged silica pore walls. Both MML and the pore walls have a net negative charge, which should lead to repulsion. Other contributing interactions may involve uncharged silanol groups on the pore walls. The silanol groups are strong hydrogen bond donors and may interact with carboxylate groups or other hydrogen bond acceptors in the enzyme. There are also van der Waals interactions between the enzyme and the silica surface.

In Paper II MPS-1000, MPS-300 and MPS-40 were used as support for MML and ROL. As shown in Section 5.1., the materials have varying particle size and morphology but they all have a pore size around 9 nm. The two lipases have the same molecular weight but widely different isoelectric points (Table 3). The protein concentration was estimated with UV adsorption at 280 nm. As can be seen in Figure 28a, the amount of immobilized MML and ROL for the three materials was very similar. This is counter to what one would anticipate considering that smaller particles mean a larger surface area, i.e., more pores exposed to the surrounding water phase, where the enzyme is present. Thus, it seems that the particle size is not an important parameter for the loading capacity within the particle size range investigated.

The immobilization was also carried out at varying pH values to investigate whether the immobilization of MML and ROL could be further improved (Figure 28b). The loading of MML increased with decreasing pH. The isoelectric point (pI) of MML is 3.8 and the point of zero charge (pzc) of silica is around 2. Therefore both the pore walls and the MML molecules carried a negative net charge in all the buffers. The largest loading was obtained at pH 5, most likely because the electrostatic repulsion between MML and silica, as well as between MML molecules, was then quite weak. The loading of ROL did not vary much with the pH. The pI of ROL is 7.6,

which means that the enzyme has a positive net charge at pH 5, 6 and 7 and is slightly negatively charged at pH 8. The lower the pH within the interval 5-7, the more pronounced is the positive net charge of ROL but the less pronounced is the negative surface charge of silica. It is therefore not obvious how the Columbic attraction between the enzyme and the silica surface will vary with pH. At pH 8 the net charge of ROL is slightly negative but the enzyme may adopt a conformation such that it exposes positively charged groups toward the silica surface or other interactions may be dominating. Similar results were observed in Paper I for BPT. Although the loading of BPT (pI 10.5) increased with increasing pH (from pH 6.0 to pH 7.6) the difference was not as pronounced as for MML (See the results in Paper I, Table 4). It is important to note that the distribution of the enzyme surface charges, and not just the net charge, may influence the interaction between enzyme and silica. Furthermore, negatively charged enzymes, like MML, may diffuse into the pores without adsorbing to the likewise negatively charged walls, whereas positively charged enzymes are likely to adsorb readily to the pore walls and thus never reach as far into the channels.

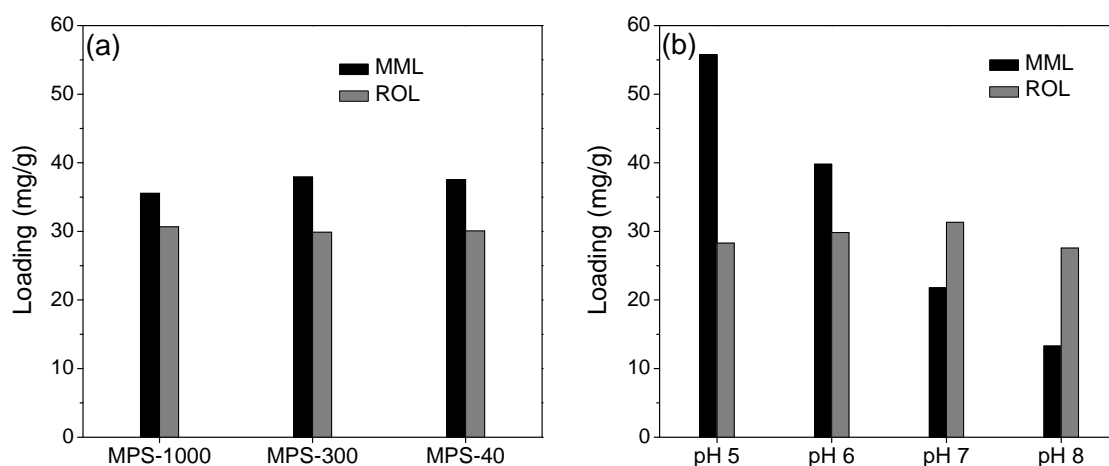


Figure 28. Immobilization of MML and ROL into (a) MPS-1000, MPS-300 and MPS-40 in phosphate buffer of pH 6 and (b) MPS-300 in phosphate buffers of pH 5, 6, 7 and 8.

The protein concentration in Paper III was determined with the Bradford assay, using BSA as a standard. The immobilization of the enzyme was rapid with the majority being immobilized during the first 10 minutes. (Figure 29 displays the decrease in protein concentration in the solution due to protein immobilization and Figure 27 displays the increase of protein in the material.) Since Depol740L is a slurry of proteins, FAE immobilization was confirmed by comparing FAE activity before and after immobilization. For MPS-9P the assay showed that 83 % of the enzyme was immobilized whereas almost no FAE activity could be detected in the solution after immobilization (See Section 3.1 in Paper III). This indicates that the immobilization of FAE was selective. For MPS-5P 39 % of the enzyme was immobilized and 45 % of the activity in the solution was lost. Thus, the immobilization into MPS-5P was not selective. It is likely that the pore size is the limiting factor for immobilization in MPS-5P and most of the enzyme will then be located on the outer particle surface.

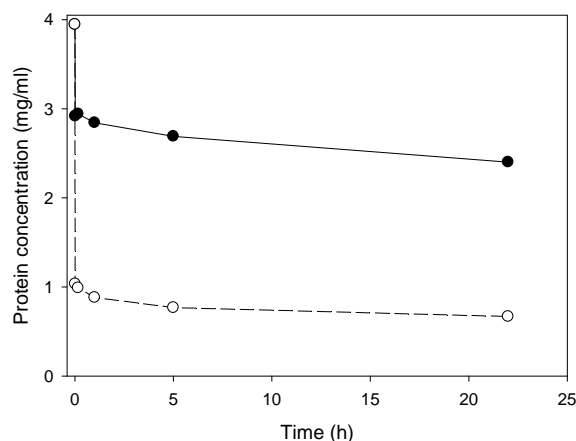


Figure 29. Immobilization rate of FAE into SBA-15 with 5 nm and 9 nm pores in MOPS buffer of pH 6.0. The plot illustrates the residual protein concentration in the solution throughout the immobilization.

5.2.2 Enzyme leakage

Throughout the activity experiments leak tests were continuously performed. Figure 30 shows the leakage of MML and ROL after 24 h at varying pH (Paper II). For MML, where both the enzyme and the pore walls are negatively charged, there is considerable leakage, particularly at the lower pH values (Figure 30a). For ROL, where one can assume attractive interactions to be dominating in this pH range there is virtually no leakage during the first 24 h (Figure 30b). Extending the time beyond 24 h gave no further leakage of any of the lipases.

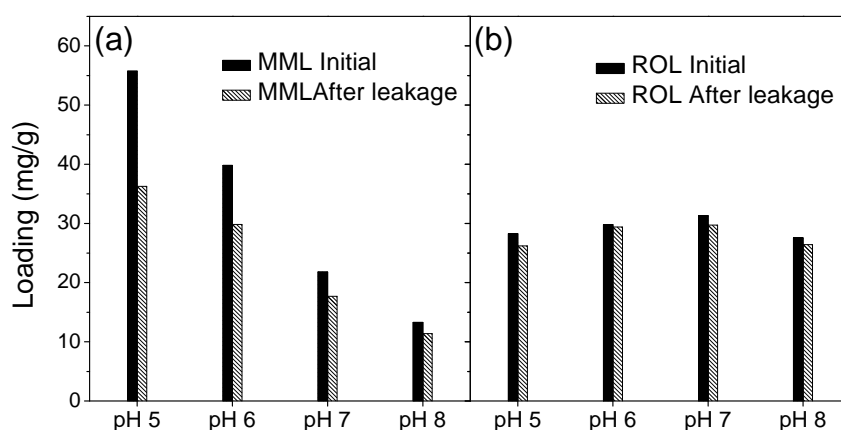


Figure 30. Amount of (a) MML and (b) ROL in MPS-300 initially and after 24 h exposure to water.

For BPT, in Paper I, around 30 % of the amount initially loaded enzyme leaked out from the MPS-5P particles. The leakage was somewhat higher from both MPS-6P and MPS-9P. The leakage mainly took place during the first 30 minutes. The relatively large leakage of BPT compared to the lipase may be explained by the large initial loading (Figure 27a). A large loading may result in a larger amount of loosely bound enzymes in the pores which are more prone to leach out. As for BPT, the leakage of MML took place within the first 30 minutes. No further loss was detected after that. The amount of MML that leaked from the particles was similar for the three materials. However, since the totally loaded amount differed between the materials

(Figure 27b) the percent leakage varied significantly; 32 % leaked from MPS-5P, 23 % from MPS-6P and 16 % from MPS-9P. A probable explanation to this is that the major leakage comes from release of enzyme molecules adsorbed on the outer surface of the particles and not from inside the pores. No leakage of FAE was detected in Paper III (See Section 5.3).

5.3 Catalytic activity of immobilized enzymes

In Paper I hydrolysis of N- α -benzoyl-DL-arginine-4-nitroanilide (BAPNA) into 4-nitroaniline was used as model reaction to test the activity of the BPT (Figure 17, Section 4.5.1). To get comparable results the immobilization time was chosen to be five hours, which was close to equilibrium for all pore sizes (see Figure 27a). Figure 31 shows the decline in product yield over time, which was attributed to deactivation of the enzyme. However, the initial rapid decrease also involves leakage during the first 30 minutes. The activity was significantly affected by the pore size. The material with medium sized pores, MPS-6P, gave both the highest yield of product and the best retention of the activity (Figure 31a). The lower product yield with MPS-5P may be explained by the lower amount of immobilized BPT in combination with the more confined environment. The smaller pores may prevent the substrate from reaching the active site. A tentative explanation to the rapid loss of activity in MPS-9P is that the pores are too large to provide the enzyme with a protected environment that retards the autocatalytic degradation. The low product yield of immobilized BPT compared to BPT free in solution (Figure 31b) was most probably due to a deactivation during the immobilization. However, limitations in substrate access inside the pores and unfavourable enzyme conformation may also be contributing factors.

Hydrolysis of 4-nitrophenyl acetate (pNPA) into 4-nitrophenol (pNP) was used as model reaction to test the activity of the immobilized lipase (Figure 16, Section 4.5.1). The effect of the pore size was even more apparent than for BTP (Figure 32). The product yield was by far the largest for MML in the largest pores, MPS-9P. As discussed in Section 3.2.1 most lipases have a lid that reveals the active site upon interfacial activation. Such a conformational change is likely to require considerable space. When comparing native MML free in solution with immobilized MML it was observed that the product formation was more than twice as large for MML in MPS-9P. This is likely due to interfacial activation of MML bound to silica. Since the prepared materials in this thesis are calcined, many of the silanol groups on the silica surface are converted into hydrophobic siloxane bridges (see Section 2.1). Hence, the silica surface will be partly hydrophobic, which may promote lipase activation.

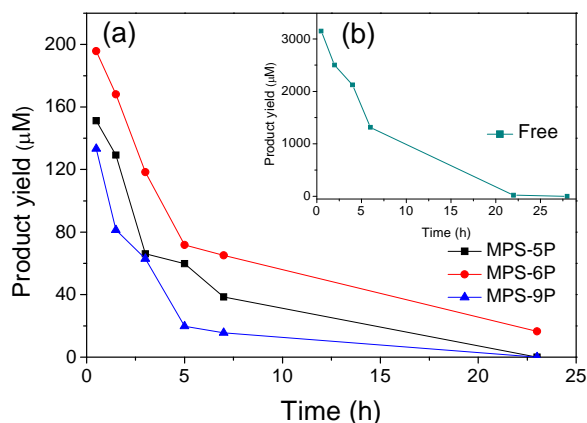


Figure 31. Concentration of produced 4-nitroaniline by a) BPT immobilized in MPS-5P, MPS-6P and MPS-9P and b) BPT free in solution. (Amount of free enzyme corresponds to the amount incorporated into MPS-9P at pH 7.6.)

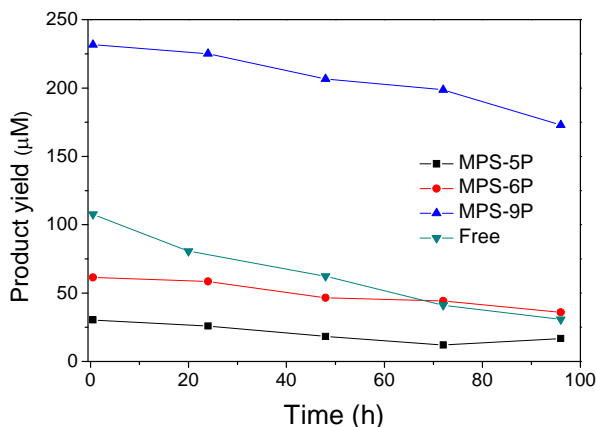


Figure 32. Concentration of produced 4-nitrophenol by lipase incorporated in (a) MPS-5P, MPS-6P and MPS-9P and by lipase free in solution. (Amount of free enzyme corresponds to the amount incorporated into MPS-9P at pH 7.6.)

In Paper II the catalytic activity of MML and ROL in the three particles with different size but with the same pore diameter, see Figures 21b-d, was compared. As shown in Section 5.2, the enzyme loading was approximately the same in the materials. However, both MML and ROL were considerably more active in MPS-300 compared to the two other materials (Figure 33). A probable explanation to the lower lipase activity in the larger MPS-1000 particles is that these particles have longer pores, which means that a smaller relative amount of enzymes are accessible to the substrate. Enzymes far down the longer pores may not be utilized. Along this way of reasoning the smallest particles, MPS-40, would provide the highest lipase activity. This was not the case, however. We believe that the relatively poor performance of MPS-40 in this respect is due to the fact that the pores, according to TEM and nitrogen physisorption, are slit-shaped and also have a much broader pore size distribution than the two other materials (Figure 24b). Even if the average pore size of MPS-40 is the same as for MPS-300 and MPS-1000, only a small fraction of the pores in MPS-40 are actually around the optimum size of 9 nm.

MPS-300 was chosen as support for the lipases in Paper II when investigating the pH dependence on loading and activity, because they had proven to give the most active lipase in the model reaction. In Figure 34 it is shown that both MML and ROL were most active when immobilized at pH 8 (MML-8 and ROL-8) and that the activity decreased with decreasing pH during the immobilization. (It should be emphasized that all activity tests were performed in a phosphate buffer of pH 7.) Figure 34 also shows that the specific activity of MML-8 was more than four times as high as of MML free in solution. The difference was much less pronounced for ROL. Surface tension measurements of the two lipases showed that MML is more surface active (47 mN/m) than ROL (60 mN/m). This indicates that MML will interact more strongly with hydrophobic patches on the silica pore walls, which could explain why its activity was more enhanced when situated inside the pores compared to ROL.

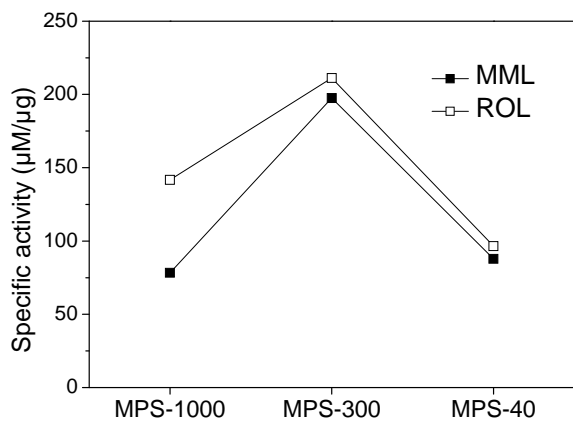


Figure 33. Comparison of the specific activity for MML and ROL (amount of product/mass of enzyme) entrapped in MPS-1000, MPS-300 and MPS-40 at pH 6.

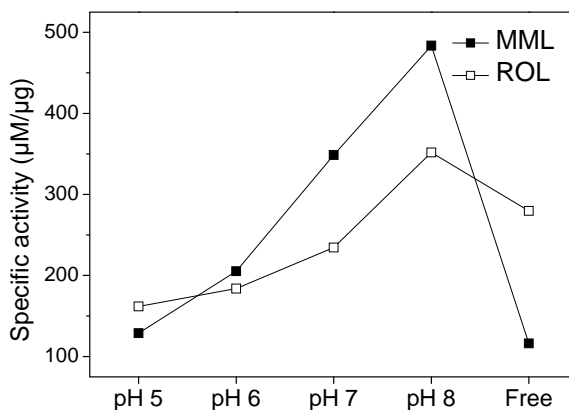


Figure 34. Comparison of the specific activity for MML and ROL in MPS-300 (amount of product/mass of enzyme) at pH 5, 6, 7 and 8.

Product yield measurements over time showed that the entrapped enzymes were quite stable (Figure 35). The slight increase that is seen for MML-8 and all samples of immobilized ROL (up to 100 h) may tentatively be explained by a rearrangement of the entrapped enzyme into a more favorable position or conformation. It can also be seen that the more than four times lower loading achieved at pH 8 compared to pH 5 for MML (see Figure 30a) was compensated by a corresponding increase in specific activity. The results point at the importance of immobilizing the enzyme in its most active state. Thus, it appears that the conformation attained during the entrapment at a certain pH is to some extent conserved after the immobilization.

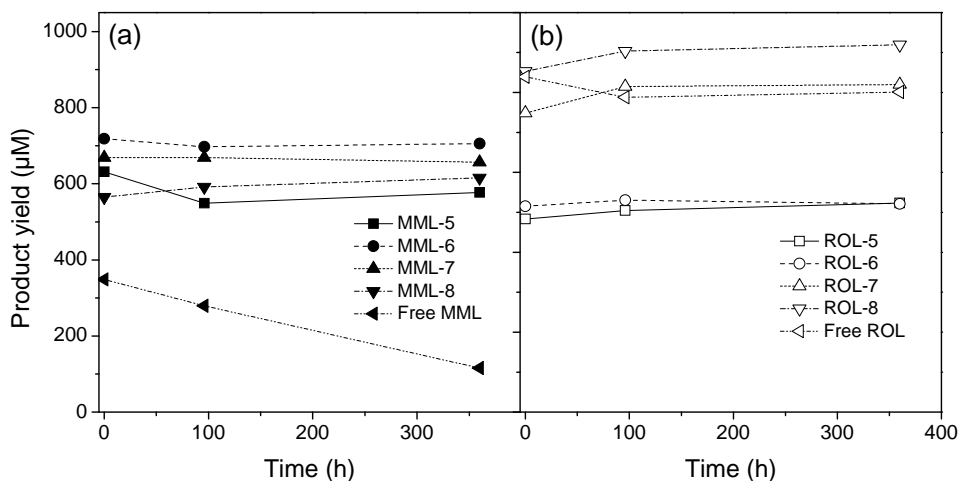


Figure 35. (a) Yield of 4-nitrophenol for (a) MML and (b) ROL entrapped in MPS-300 at pH 5, 6, 7 and 8 and free in solution.

In Paper III the transesterification reaction of methyl ferulate (MFA) with 1-butanol into butyl ferulate (BFA) was used as a model reaction for the immobilized enzyme (See Figure 1 in Paper III). Figure 36 shows that FAE immobilized into MPS-9P resulted in significantly higher transesterification yield compared to MPS-5P. FAE immobilized into MPS-9P was also 3.5 times more active in terms of specific transesterification activity (See Table 2 in Paper III). The larger

space for the enzyme in MPS-9P may explain the higher activity compared to when the enzyme was immobilized in MPS-5P. A better substrate access in the 9 nm pores may also be a contributing factor. Comparing the initial activity of MPS-9P with that of free enzyme, 40 % of the specific BFA activity was lost. However, a significantly higher overall yield was obtained when the enzyme was immobilized in the MPS-9P material and this enzyme preparation also retained the activity better throughout the reaction.

The hydrolysis of MFA into ferulic acid (FA) was also quantified and the product selectivity, defined by the BFA/FA molar ratio, was compared. Under normal conditions FAE hydrolyses the ester bond to yield FA and an alcohol. However, in this study, it was observed that the immobilized enzyme consistently generated less FA (higher BFA/FA ratio) than was the case for the free enzyme (Figure 37). The BFA/FA ratios in the reactions with the enzyme entrapped into MPS-5P and MPS-9P were very similar, thus independent of pore size. It is more likely that the higher BFA/FA ratio for immobilized enzyme compared to the free enzyme is related to the enzyme being adsorbed to the silica surface rather than a confining effect of the pore. This hypothesis was confirmed by immobilizing Depol740L onto non-porous silica particles, which gave a similar BFA yield as with MPS-9P. It remains to determine whether this phenomenon is due to a conformational change of the enzyme or a favorable arrangement of water and butanol molecules on the silica surface. Important to note is that also other proteins and enzymes in the crude Depol740L preparation may influence the FAE activity.

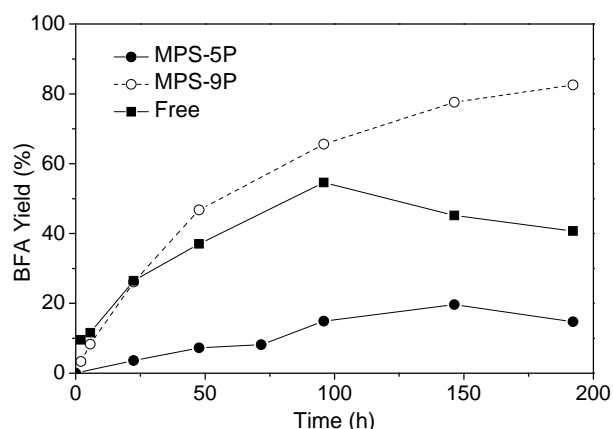


Figure 36. Transesterification of MFA (20 mM) into BFA over time in 7.5 % water for MPS-5P, MPS 9P, and free enzyme (amount of free enzyme corresponds to the amount immobilized into MPS-5P).

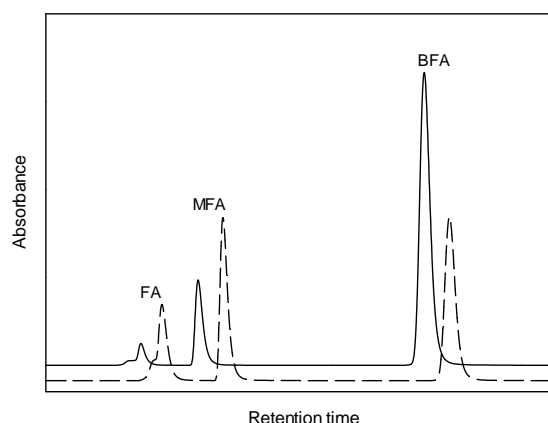


Figure 37. Typical HPLC chromatogram illustrating the higher BFA/FA molar ratio of immobilized enzyme (solid line) compared to free enzyme (dashed line). Retention times for FA, MFA and BFA were 1.0, 1.5 and 3.0 min, respectively.

Immobilized FAE was relatively stable throughout 6 runs, retaining 70% and 96% of their activities compared to the first run for MPS-5P and MPS-9P, respectively. The better reusability of MPS-9P can partly be explained by the large BFA yield (~85%), where a decrease in activity will not be as easily noticeable as for MPS-5P with a significantly lower yield (15–20%). Another explanation can be that the enzymes in MPS-9P are conformationally stabilized inside the pores by protein–silica surface interactions and enzyme confinement, as described previously for other

enzymes [79,80]. No activity could be detected in the supernatant, indicating that the slow decrease in activity of the immobilized enzyme is mainly due to inactivation of the enzyme and not leakage. This suggests that the interaction to the silica surface is strong under the conditions used in the study.

Chapter 6

CONCLUDING REMARKS AND FUTURE WORK

The main objective in this thesis was to study the immobilization of enzymes in mesoporous silica materials. Mesoporous silica is a promising material as support for enzymes due to the large surface area and the well-ordered and uniform pores with an adjustable pore size in a suitable size range. The results presented showed that optimal performance of immobilized enzymes, regarding loading, catalytic activity and stability is dependent on both the properties of the mesoporous silica and the enzyme characteristics. Not only the size and the surface properties of the enzyme but also the characteristics of the active site are decisive. Furthermore, the optimal conditions depend on which type of improved performance one is striving for. Is the goal enhanced stability, increased enzymatic activity, altered enzymatic activity or a combination of these? Consequently, the ideal conditions are specific for each enzyme and purpose.

In Paper I trypsin from *bovine pancreas* (BPT) was immobilized giving a relatively large loading amount. For trypsin, autocatalytic degradation is a major issue for the long term stability. It was found that a relatively narrow pore size is preferred over a larger pore size probably because a confined environment provides better protection towards degradation. However, a too narrow pore size results in a slower immobilization rate and the enzyme may adopt an unfavorable conformation. Access of the substrate may also be hindered if the pores are narrow. The immobilization rate of lipase from *Mucor miehei* (MML) was slow compared to immobilization of BPT and a considerably lower loading was obtained. Due to the lid that covers the active site of most lipases, a larger space is needed in order for the enzyme to fold into an active state. It was shown that a lipase immobilized in mesoporous silica can be more active compared to lipase free in solution. It is likely that the silica surface contributed to the interfacial activation of the lipase.

When immobilizing lipase from *Rhizopus oryzae* (ROL) and MML into the pores of the three particle types in Paper II it was found that the loading did not differ significantly. Thus, it seems that the particle size is not an important parameter for the loading capacity within the particle size range studied. However, the specific activity was clearly affected by the particle size. Both lipases were most active when immobilized into the 300 nm particles. The fact that MML, but not ROL to the same extent, became much more active when entrapped in the pores than free in solution may be due to MML being more surface active than ROL. MML may therefore interact more strongly with the relatively hydrophobic pore walls.

For feruloyl esterases (FAE), in Paper III, immobilization caused a desired altered enzymatic activity towards transesterification of butyl ferulate while less hydrolysis product was generated, resulting in higher transesterification yield compared to when the free enzyme was used. The immobilization was rapid and the stability and reusability was good for FAE.

The loading of an enzyme can be improved by finding the most optimal pH. However, a favourable pH regarding loading does not always coincide with an optimal pH for good specific activity. The results in Paper II point at the importance of immobilizing the enzymes in their most active state.

There is still a lack of knowledge with regard to the adsorption process into the pores. More studies must be performed to gain understanding in how various types of enzymes (or other proteins), which differ in isoelectric point, mass and structure, are immobilized into mesoporous materials. For this purpose quartz crystal microbalance with dissipation (QCM-D) seems to be a suitable technique. QCM-D is an ultrasensitive weighing device, capable of measuring mass changes in the nanogram range in real time and at the same time monitor the elastic and viscoelastic properties of the adsorbed molecules. Preliminary studies have been performed, where mesoporous particles and non-porous particles were successfully attached to silica-coated crystals using silane linkers. The enzyme immobilization on mesoporous silica particles, non-porous silica particles and flat silica surfaces will be compared using buffers of various pH.

ACKNOWLEDGEMENT

The Swedish Research Council is acknowledged for financial support.

I would also like to thank the following people:

First of all, my supervisor, Krister Holmberg, for giving me the opportunity to do research at Applied Surface Chemistry and for all your invaluable support and advice.

My co-supervisor, Lisbeth Olsson, and the other members of the SUPRA enzyme cluster: Christian Thörn, Nils Carlsson, Björn Åkerman and Krister for a great collaboration and inspirational meetings.

My co-authors Emma Johansson (Linköping University) and Christian Thörn.

My former diploma worker, Albert Barrabino, for contributing to the project.

Martin Andersson for all help with the TEM and SEM and for giving me the opportunity to go to MAX-lab.

All the people at TYK for creating such a nice working environment, especially in the coffee room. Special thanks to Maria, Emma, Alex, Jonathan, Johan, Markus, Daniel, Ralph, Björn, Adriana, Ali, Åsa, Zebastian, Freddy and Christoffer for making it fun at work and off-work. And of course, the world's greatest innebandy crew for making it easy getting up on Wednesday mornings!

Finally, I would like to thank my wonderful friends (especially Camilla, Emma and Sari) and my beloved family for always supporting me and believing in me, no matter what. My dear fiancé, Mattias, for your endless love and patience. I look forward to our future together.

REFERENCES

- [1] Ahuja, S. K., Ferreira, G. M. & Moreira, A. R. *Crit. Rev. Biotechnol.* 24, (2004) 125.
- [2] Koeller, K. M. & Wong, C. H. *Nature* 409, (2001) 232.
- [3] Nagayasu, T., Miyanaga, M., Tanaka, T., Sakiyama, T. & Nakanishi, K. *Biotechnol. Bioeng.* 43, (1994) 1118.
- [4] Carrea, G. & Riva, S. *Angew Chem Int Edit* 39, (2000) 2226.
- [5] Powell, K. A., Ramer, S. W., del Cardayre, S. B., Stemmer, W. P. C., Tobin, M. B., Longchamp, P. F. & Huisman, G. W. *Angew Chem Int Edit* 40, (2001) 3948.
- [6] Wang, P., Dai, S., Waezsada, S. D., Tsao, A. Y. & Davison, B. H. *Biotechnol. Bioeng.* 74, (2001) 249.
- [7] Tischer, W. & Kasche, V. *Trends Biotechnol.* 17, (1999) 326.
- [8] Fernandez-Lafuente, R., Armisen, P., Sabuquillo, P., Fernández-Lorente, G. & M. Guisán, J. *Chem. Phys. Lipids* 93, (1998) 185.
- [9] Bornscheuer, U. T. *Angew Chem Int Edit* 42, (2003) 3336.
- [10] Hartmann, M. *Chem. Mater.* 17, (2005) 4577.
- [11] Beck, J. S., Vartuli, J. C., Roth, W. J., Leonowicz, M. E., Kresge, C. T., Schmitt, K. D., Chu, C. T. W., Olson, D. H. & Sheppard, E. W. *J. Am. Chem. Soc.* 114, (1992) 10834.
- [12] Zhao, D. Y., Feng, J. L., Huo, Q. S., Melosh, N., Fredrickson, G. H., Chmelka, B. F. & Stucky, G. D. *Science* 279, (1998) 548.
- [13] Yang, P. D., Zhao, D. Y., Margolese, D. I., Chmelka, B. F. & Stucky, G. D. *Nature* 396, (1998) 152.
- [14] Zhao, D. Y., Huo, Q. S., Feng, J. L., Chmelka, B. F. & Stucky, G. D. *J. Am. Chem. Soc.* 120, (1998) 6024.
- [15] Kartini, I., Meredith, P., da Costa, J. C. D., Riches, J. D. & Lu, G. Q. M. *Curr Appl Phys* 4, (2004) 160.
- [16] Yanagisawa, T., Shimizu, T., Kuroda, K. & Kato, C. *Bull. Chem. Soc. Jpn.* 63, (1990) 988.
- [17] Kresge, C. T., Leonowicz, M. E., Roth, W. J., Vartuli, J. C. & Beck, J. S. *Nature* 359, (1992) 710.
- [18] Slowing, I. I., Trewyn, B. G. & Lin, V. S. Y. *J. Am. Chem. Soc.* 129, (2007) 8845.
- [19] Vallet-Regi, M., Ramila, A., del Real, R. P. & Perez-Pariente, J. *Chem. Mat.* 13, (2001) 308.
- [20] Han, Y. J., Stucky, G. D. & Butler, A. *J. Am. Chem. Soc.* 121, (1999) 9897.
- [21] Sayari, A. *Chem. Mater.* 8, (1996) 1840.
- [22] Yiu, H. H. P. & Wright, P. A. *J. Mater. Chem.* 15, (2005) 3690.
- [23] Deere, J., Magner, E., Wall, J. G. & Hodnett, B. K. *J. Phys. Chem. B* 106, (2002) 7340.
- [24] Díaz, J. F. & Balkus, K. J. *J. Mol. Cat. B: Enzym.* 2, (1996) 115.
- [25] Beck, J. S., Vartuli, J. C., Roth, W. J., Leonowicz, M. E., Kresge, C. T., Schmitt, K. D., Chu, C. T. W., Olson, D. H., Sheppard, E. W., Mccullen, S. B., Higgins, J. B. & Schlenker, J. L. *J. Am. Chem. Soc.* 114, (1992) 10834.
- [26] Holmberg, K., Jönsson, B., Kronberg, B. & Lindman, B. (2003). Surfactants and Polymers in Aqueous Solution. In *Surfactants and Polymers in Aqueous Solution*, pp. i. John Wiley & Sons, Ltd.
- [27] Hench, L. L. & West, J. K. *Chem. Rev. (Washington, DC, U. S.)* 90, (1990) 33.
- [28] Zhao, D. Y., Sun, J. Y., Li, Q. Z. & Stucky, G. D. *Chem. Mater.* 12, (2000) 275.
- [29] Yu, C., Fan, J., Tian, B., Zhao, D. & Stucky, G. D. *Advanced Materials* 14, (2002) 1742.
- [30] Yokoi, T., Sakamoto, Y., Terasaki, O., Kubota, Y., Okubo, T. & Tatsumi, T. *J. Am. Chem. Soc.* 128, (2006) 13664.
- [31] Yu, C., Fan, J., Tian, B. & Zhao, D. *Chem. Mat.* 16, (2004) 889.

- [32] Boissiere, C., Larbot, A., van der Lee, A., Kooyman, P. J. & Prouzet, E. *Chem. Mater.* 12, (2000) 2902.
- [33] Ruggles, J. L., Gilbert, E. P., Holt, S. A., Reynolds, P. A. & White, J. W. *Langmuir* 19, (2003) 793.
- [34] Galarneau, A., Cambon, H., Di Renzo, F. & Fajula, F. *Langmuir* 17, (2001) 8328.
- [35] Kocherbitov, V. & Alfredsson, V. *J. Phys. Chem. C* 111, (2007) 12906.
- [36] Zhao, X. S., Lu, G. Q., Whittaker, A. K., Millar, G. J. & Zhu, H. Y. *J. Phys. Chem. B* 101, (1997) 6525.
- [37] Bae, Y. K. & Han, O. H. *Micropor. Mesopor. Mater.* 106, (2007) 304.
- [38] Nandiyanto, A. B. D., Kim, S.-G., Iskandar, F. & Okuyama, K. *Micropor. Mesopor. Mater.* 120, (2009) 447.
- [39] Lettow, J. S., Han, Y. J., Schmidt-Winkel, P., Yang, P., Zhao, D., Stucky, G. D. & Ying, J. Y. *Langmuir* 16, (2000) 8291.
- [40] Flodstrom, K., Wennerstrom, H. & Alfredsson, V. *Langmuir* 20, (2004) 680.
- [41] Flodstrom, K., Teixeira, C. V., Amenitsch, H., Alfredsson, V. & Linden, M. *Langmuir* 20, (2004) 4885.
- [42] Linton, P., Hernandez-Garrido, J.-C., Midgley, P. A., Wennerstrom, H. & Alfredsson, V. *Phys. Chem. Chem. Phys.* 11, (2009) 10973.
- [43] Sayari, A., Han, B.-H. & Yang, Y. *J. Am. Chem. Soc.* 126, (2004) 14348.
- [44] Johansson, E. M., Cordoba, J. M. & Oden, M. *Micropor. Mesopor. Mater.* 133, (2010) 66.
- [45] Johansson, E. M., Ballem, M. A., Córdoba, J. M. & Odén, M. *Langmuir* 27, (2011) 4994.
- [46] Wang, Y. G., Zhang, F. Y., Wang, Y. Q., Ren, J. W., Li, C. L., Liu, X. H., Guo, Y., Guo, Y. L. & Lu, G. Z. *Mater. Chem. Phys.* 115, (2009) 649.
- [47] Kirk, O., Borchert, T. V. & Fuglsang, C. C. *Curr. Opin. Biotechnol.* 13, (2002) 345.
- [48] Malhotra, B. D. & Chaubey, A. *Sensor Actuat B-Chem* 91, (2003) 117.
- [49] Kallenberg, A. I., van Rantwijk, F. & Sheldon, R. A. *Adv. Synth. Catal.* 347, (2005) 905.
- [50] Jing, H., Li, X. F., Evans, D. G., Duan, X. & Li, C. Y. *J Mol Catal B-Enzym* 11, (2000) 45.
- [51] Matuszewska, B., Norde, W. & Lyklema, J. *J. Colloid Interface Sci.* 84, (1981) 403.
- [52] Lyklema, J. *Colloids Surf.* 10, (1984) 33.
- [53] Hudson, S., Magner, E., Cooney, J. & Hodnett, B. K. *The Journal of Physical Chemistry B* 109, (2005) 19496.
- [54] Fan, J., Lei, J., Wang, L., Yu, C., Tu, B. & Zhao, D. *Chem. Commun.*, (2003) 2140.
- [55] Takahashi, H., Li, B., Sasaki, T., Miyazaki, C., Kajino, T. & Inagaki, S. *Micropor. Mesopor. Mater.* 44, (2001) 755.
- [56] Sasaki, T., Kajino, T., Li, B., Sugiyama, H. & Takahashi, H. *Appl. Environ. Microbiol.* 67, (2001) 2208.
- [57] Lee, C. H., Lang, J., Yen, C. W., Shih, P. C., Lin, T. S. & Mou, C. Y. *J. Phys. Chem. B* 109, (2005) 12277.
- [58] Lei, C. H., Shin, Y., Liu, J. & Ackerman, E. J. *Nano Lett.* 7, (2007) 1050.
- [59] Sharma, R., Chisti, Y. & Banerjee, U. C. *Biotechnol Adv* 19, (2001) 627.
- [60] Brady, L., Brzozowski, A. M., Derewenda, Z. S., Dodson, E., Dodson, G., Tolley, S., Turkenburg, J. P., Christiansen, L., Huge-Jensen, B., Norskov, L., Thim, L. & Menge, U. *Nature* 343, (1990) 767.
- [61] Wu, X., Jääskeläinen, S. & Linko, W.-Y. *Appl. Biochem. Biotechnol.* 59, (1996) 145.
- [62] Hiol, A., Jonzo, M. D., Rugani, N., Druet, D., Sarda, L. & Comeau, L. C. *Enzyme Microb. Technol.* 26, (2000) 421.
- [63] Gupta, R., Beg, Q. K. & Lorenz, P. *Appl. Microbiol. Biotechnol.* 59, (2002) 15.
- [64] Polgar, L. *Cell. Mol. Life Sci.* 62, (2005) 2161.
- [65] Fazary, A. E. & Ju, Y. H. *Acta Bioch Bioph Sin* 39, (2007) 811.
- [66] Topakas, E., Vafiadi, C. & Christakopoulos, P. *Process Biochem.* 42, (2007) 497.

- [67] Murakami, A., Nakamura, Y., Koshimizu, K., Takahashi, D., Matsumoto, K., Hagihara, K., Taniguchi, H., Nomura, E., Hosoda, A., Tsuno, T., Maruta, Y., Kim, H. W., Kawabata, K. & Ohigashi, H. *Cancer Lett* 180, (2002) 121.
- [68] Kikuzaki, H., Hisamoto, M., Hirose, K., Akiyama, K. & Taniguchi, H. *J. Agric. Food Chem.* 50, (2002) 2161.
- [69] Topakas, E., Stamatidis, H., Mastihobova, M., Biely, P., Kekos, D., Macris, B. J. & Christakopoulos, P. *Enzyme Microb. Technol.* 33, (2003) 729.
- [70] Brunauer, S., Emmett, P. H. & Teller, E. *J. Am. Chem. Soc.* 60, (1938) 309.
- [71] Barrett, E. P., Joyner, L. G. & Halenda, P. P. *J. Am. Chem. Soc.* 73, (1951) 373.
- [72] Sing, K. S. W., Everett, D. H., Haul, R. A. W., Moscou, L., Pierotti, R. A., Rouquerol, J. & Siemieniewska, T. *Pure Appl. Chem.* 57, (1985) 603.
- [73] Lowry, O. H., Rosebrough, N. J., Farr, A. L. & Randall, R. J. *J. Biol. Chem.* 193, (1951) 265.
- [74] Smith, P. K., Krohn, R. I., Hermanson, G. T., Mallia, A. K., Gartner, F. H., Provenzano, M. D., Fujimoto, E. K., Goeke, N. M., Olson, B. J. & Klenk, D. C. *Anal. Biochem.* 150, (1985) 76.
- [75] Bradford, M. M. *Anal. Biochem.* 72, (1976) 248.
- [76] Wiechelman, K. J., Braun, R. D. & Fitzpatrick, J. D. *Anal. Biochem.* 175, (1988) 231.
- [77] Fordham, S. *Proc R Soc Lon Ser-A* 194, (1948) 1.
- [78] Stauffer, C. E. *J. Phys. Chem.* 69, (1965) 1933.
- [79] Ravindra, R., Shuang, Z., Gies, H. & Winter, R. *J. Am. Chem. Soc.* 126, (2004) 12224.
- [80] Urabe, Y., Shiomi, T., Itoh, T., Kawai, A., Tsunoda, T., Mizukami, F. & Sakaguchi, K. *ChemBioChem* 8, (2007) 668.

